ON THE PERFORMANCE OF THE ECMWF MODEL IN THE TROPICS

W. A. Heckley

European Centre for Medium Range Weather Forecasts,
Shinfield Park, Reading, U.K.

A B S T R A C T

The ECMWF forecasting system is briefly described. Examination of its monthly mean performance indicates reasonable skill in the prediction of wind fields and precipitation in at least the first two days of the forecast. Thereafter the precipitation tends towards a climatological distribution. Serious difficulties are apparent early in the forecasts in the maintenance of the quasi-stationary large scale flow in the tropics. These problems are related to erroneous forcing of a few large scale modes. The sensitivity of an individual forecast to modified forcing is briefly illustrated.

1. INTRODUCTION

This contribution discusses some aspects of the mean performance of the ECMWF forecasting model in the tropics. It is not intended to be a comprehensive review nor does it attempt a comparison with results from other groups. A review of the performance of other models in the tropics may be found in GARP Report No. 20 (ICSU/WMO, 1978), Gilchrist (1977), Gilchrist et al. (1980), Rowntree (1978) and Heckley (1981). Instead it tries to convey an overall impression of the capability of the model and to highlight some of what are felt to be its principal problems. The discussion is mainly based upon monthly means of operational ten-day forecasts. These forecasts are global and are produced routinely each day. Some individual forecasts and longer integrations are also discussed where necessary to emphasise particular aspects.

A brief introduction to the ECMWF forecasting system is given in the next section. This is followed by a discussion of the mean performance of the model in terms of its ability to forecast tropical precipitation. This is followed by a discussion of the ability of the model to simulate the Indian Summer Monsoon. Section 5 discusses the model's ability to maintain the trade wind circulations. Section 6 discusses the model's divergent circulations. Finally, Section 7 describes the flow changes in the early stages of the forecasts and relates them to idealized theoretical models.

The following results should be considered in the light that they are obtained from a model capable of producing what is generally considered to be useful forecasts out to about five to seven days in the extra-tropics and, by the same considerations, about one or two days in the tropics.

2. THE ECMWF GLOBAL FORECASTING SYSTEM

A global forecasting system has two major components, namely the data assimilation and the prediction model. Although these two components can be set up independently, they are mutually dependent and highly integrated in the ECMWF system. This system is outlined in Fig. 1.

2.1 The data assimilation

The irregularity of atmospheric observations and the requirement of a well-balanced initial state for the forecast model has lead to the use of a three-dimensional multi-variate analysis scheme which simultaneously analyses the mass and wind fields (Lorenc, 1981). An additional advantage of this scheme

is that it provides a consistent way of checking the data. This has made it possible to establish an essentially automatic operational procedure at ECMWF, and no manual intervention during the analysis process is carried out. Analyses are performed every 6 hours with observations used in a 6-hour "time-window". The model provides the necessary "first guess" for the analysis which in turn provides the initial state for the 6-hour forecasting step required to produce the first guess for the following analysis.

The dynamical balance in the analysis is not sufficiently good to include spurious inertia-gravity oscillations, these are large enough to have a significant influence on the subsequent acceptance of data when a 6-hour forecast is used as the "first guess" for the next analysis. This is partly overcome by use of a non-linear normal-mode initialization (Temperton and Williamson, 1981; Williamson and Temperton, 1981). The present scheme is applied using adiabatic non-linear tendencies in the iterative procedure, and as a result initial vertical velocities are seriously damped in tropical regions. Modifications to remedy this defect are under development.

Anomalous surface conditions may be of particular importance in forcing atmospheric anomalies in the tropics, and it is thus appropriate to note here the initial values used for surface fields. Sea-surface temperature, soil moisture and albedo are assigned climatological initial values. Land temperature and snow cover are derived from the forecast model used in the data assimilation cycles, although the snow cover is reset monthly to climatology. Analysis schemes for some of these surface fields are currently under development.

2.2 The forecast model

The numerical model described is the model chosen for the first phase of operational forecasting at ECMWF, which uses a finite-difference scheme based on a staggered grid of variables known as the C-grid (Arakawa and Lamb, 1977). Choice of this grid was made mainly because of its low computational noise and the ease of implementation of a semi-implicit time scheme. Following the work of Arakawa (1966) and Sadourny (1975), the finite difference scheme was designed to conserve potential enstrophy during vorticity advection by the horizontal flow. Further detail has been given by Burridge and Haseler (1977), and Burridge (1979).

Vertical and horizontal resolutions for this model were selected, within overall computational constraints, to provide a reasonable description of the fundamental large-scale instabilities, some representation of the stratosphere, and an explicit boundary-layer structure. The related parameterization scheme (Tiedtke et al., 1979) describes the interactions thought to be of importance in the medium range, including a full hydrological cycle, a relatively detailed stability-dependent representation of boundary and free-atmospheric turbulent fluxes, and an interaction between the radiation and model-generated clouds.

Specific comment is required concerning two aspects of the parameterization scheme. The first is that all results to be presented were obtained using a forecast model which included no representation of the diurnal radiative cycle which in reality is an important influence on tropical precipitation. Incorporation of this cycle is currently under test. The second is that while the climatological albedo patterns include inhomogeneities of surface characteristics, the parameterization of surface evaporation and soil moisture content takes such inhomogeneities explicitly into account only in so far as they influence the drag coefficient. Results thus cannot fully represent some of the local processes, for example those involving the effect of vegetation type on evapotranspiration, which may influence rainfall.

3. FORECASTING OF TROPICAL PRECIPITATION - MEAN PERFORMANCE

Verification of rainfall forecasts in the tropics presents problems in itself. There is little data over the land areas and virtually no data over the oceans. Exceptions to this are South America, India and Indonesia. In order to smooth out some of the intrinsic variability of the rainfall it was decided to examine monthly means, and to smooth the data over a 3.75° grid. Shown in Fig. 2 are zonal means of the monthly mean rainfall for February, March and April, 1981. The units are mm/day. The thin solid line refers to the 24h forecast, the dashed line the 48h forecast, the dashed-dotted line the 120h forecast and the dotted line the 240h forecast. For comparison, the climatic values calculated by Jaeger, 1976, are indicated as a thick solid line. The seasonal march of the equatorial trough is clearly evident in the zonal means. Comparing the forecasts with climate the most obvious differences are too much rain forecast in the northern hemisphere extra-tropics and $\sim$20% too little rain forecast near to the equator. The differences in the northern hemisphere extra-tropics occur largely over the oceanic areas, however, Jaeger's climatic data over oceanic regions is possibly inaccurate. The climatic values for the Southern Ocean are questionable due

to the lack of any real data. Little systematic relation is seen between rainfall amounts and forecast length, in the zonal mean, except perhaps in April where there appears to be a decrease in forecast rainfall with time around 20^{o} to 50^{o}N. Apart from the seasonal shift, the February and March zonal means have a very similar character. The differences in April could be associated with the changes in the model orography introduced on April 1, 1981.

Figures 3 to 6 show the 24-hour monthly mean rainfall amounts for the 24-hour, 48-hour, 120-hour and 240-hour forecasts for March 1981. The principal features of the 24-hour forecast are an intense band of rain orientated NW to SE in the Central Pacific with over 16 mm/day, widespread rain of over 8 mm/day over Colombia and Brazil, heavy rain of over 16 mm/day over Central Africa, Sudan and Ethiopia, heavy rain of over 8 mm/day over southern China, and heavy rain in the Indian Ocean. At day two the pattern is very similar to day one. The areas of heavy rain noted in the 24-hour forecast have, in general, intensified and become more widespread; an exception to this is the rainfall over southern China which has weakened. By day five the geographical distribution is beginning to change and the rainfall maxima over the Pacific, South America and Central Africa are weaker. The band of rain in the Pacific has decreased to 6 mm/day; the rainfall over South America is similar to the one day forecast. There has been a slight intensification of the rainfall over Tibet. The pattern continues to change and by day ten there is no longer any sign of the intense NW to SE band of rain in the Pacific. Over the oceans the rainfall at this time occurs along the ITCZ with the heaviest rain over the Indonesian region. Over land the heaviest rainfall occurs over Venezuela, Colombia, Peru, Central Brazil, Central Africa, Madagascar and Tibet.

As already mentioned, verification of rainfall in the tropics presents something of a problem, as a rough guide we can compare the monthly means with climate. Fig. 7 shows the climatic rainfall for March reproduced from Jaeger's data. Compared with Figs. 3 to 6 it is clear that the forecast rainfall bears more and more resemblance to the climatological distribution as forecast length increases. The resemblance between the ten-day forecast (Fig. 6) and climatology, ignoring the Southern Ocean, is quite striking. The most obvious difference is the band of rain extending from Central Africa to Brazil which is missing in the forecasts, and the under prediction of rainfall in the Indonesian, western Pacific region.

Fig. 8 shows the monthly mean outgoing longwave radiation (Wm^{-2}) derived from NOAA Satellite data for March, 1981. Areas with less than 250 Wm^{-2} are shaded; these "cloudy" areas correspond closely with the areas of maximum forecast rainfall in the one or two day forecasts. Note the NW to SE orientated band of cold clouds in the Pacific coincident with the forecast rainfall. Also worth noting is the absence of cold clouds in the band from Central Africa to Brazil across the equatorial Atlantic, which lends support to the lack of forecast rainfall compared to climatology in this region.

We have seen that in the monthly mean the forecast rainfall in the tropics is (at least qualitatively) quite well predicted for the first one or two days of the forecast and thereafter tends towards the climatological distribution. This suggests that the model is responding to the imposed climatological surface fields. In order to obtain a more quantitative measure of the quality of the forecast rainfall, the rainfall reports for South America for March 1981 were averaged to obtain the monthly mean shown in Fig. 9. The large numbers refer to the forecast rainfall in tenths of mm/day for the mean of the one-day forecasts and the small numbers refer to the observed rainfall in tenths of mm/day. The areas with observed rainfall greater than 8mm/day have been outlined with a dashed line and with a solid line for forecast rain. The areas do not coincide exactly but there is a broad agreement. The most obvious differences appear in Colombia where there is an underprediction of rainfall on the western side of the Andes and an over-prediction on the eastern side. There is also an overprediction of rainfall over the Bolivian Plateau. Over most of Brazil the differences do not have a consistent sign and the rainfall (given the localised nature of tropical rainfall) is well predicted.

4. REPRESENTATION OF THE INDIAN SUMMER MONSOON

The results described in this section were obtained by Adrian Simmons and described in more detail in Simmons (1982,a).

A principal requirement of a forecasting model in the tropics is that it should be able to simulate the monsoonal circulations, these being the most significant seasonal events in the tropics. As shown by Simmons (1982, a), a characteristic deficiency of the model representation of the monsoon is a tendency for a too strong low-level flow, and particularly a too strong southerly component, over the Bay of Bengal. This is particularly marked in Fig. 10, while Fig. 11 shows that there is a corresponding erroneously-strong north-easterly flow over the same region at 200 mb. The same low-level error is evident (Fig. 12) in a 50-day integration.

In investigations of the simulated rainfall produced during a 50-day integration (Simmons, 1982, a), relatively large maximum amounts of precipitation were noted. Precipitation amounts in the first few days of the operational forecasts, during the monsoon, also appear large to the north-east of the Bay of Bengal. From the type of linear, steady model of tropical circulations examined by Gill (1980) and Simmons (1982, b) the erroneous monsoon flow can be related to excessive latent heating associated with excessive precipitation. Fig. 13 presents one such linear, steady solution in which a localized, externally-imposed heating, which is a maximum at the 400 mb level at 95°E, 20°N, is balanced by adiabatic cooling associated with upward vertical motion. The related vortex stretching and shrinking drives the illustrated horizontal flow which is characterized by south-westerly low-level and north-easterly upper-level winds in the vicinity of the heating region. In reality, and in more complete numerical models, the situation will, of course, be more complicated, particularly as the precipitation and thus the latent heating will vary with the direction and intensity of the monsoon flow.

A number of integrations have been performed to investigate the sensitivity of this particular deficiency of the forecasting system. Fig 14 shows that the problem arises(though more or less severely) for three different parameterizations of convection. In all these schemes, however, an unstable atmosphere leads to parameterized heating profiles being introduced into the model with no associated (dynamically-balancing) change to the wind field. This can result in the convective heating being largely balanced by adiabatic cooling due to excessive upward motion, rather than by a stabilizing temperature change. Thus regions of strong convection appear to persist unrealistically, with unrealistic related rainfall and circulation patterns.

5. MAINTENANCE OF THE TRADE WIND CIRCULATIONS

This discussion will only deal with the Atlantic trades, but it should be noted that similar problems occur in the Pacific and these will be discussed in more detail in section 7. Fig. 15 shows the operational analysis for the wind field at 1000 mb and 850 mb, once again, this is a monthly mean for March 1981. There is little discernable difference between the initialized and uninitialized analyses so only the initialized analysis is shown. The 24, 48, 120 and 240 hour forecasts are shown in Figs. 15 to 19. At 1000 mb the trade winds along the north west and south west coasts of Africa are well maintained throughout the forecast. Nearer the equator, the air moving north-westwards in the analysis is forecast to move north-eastwards. This turning of the wind over the Gulf of Guinea towards the African continent evident in the forecast is

presumably related to the over-intense forecast convergence over Africa. Another feature of the forecast at 1000 mb is a steady weakening throughout the forecast of the anti-cyclonic circulation in the North Atlantic and in the South Atlantic.

At 850 mb the errors are larger and more obvious. At day 1 the forecast predicts westerly winds of 8 ms^{-1} over Central Africa where the analysis shows no wind at all. The errors over this region do not intensify with time as they do at 1000 mb, in fact they decrease slowly, at day ten the wind in this region has reduced to 4 ms^{-1}. As discussed in the next section, the error in the velocity potential field also decreased steadily between days one and ten in this region. The growing error at 850 mb is a weakening of the anti-cyclonic circulation in the North Atlantic and in the South Atlantic, as at 1000 mb.

In brief, there appear to be two kinds of error associated with the tropical wind field in this region. The first, which has a very large immediate effect at 850 mb, and a smaller but amplifying effect at 1000 mb, seems to be associated with an over intense divergent circulation over Africa. The divergent wind is directly opposed to the trade wind circulation off West Africa. As discussed in the next section, this becomes less of a problem as the velocity potential field weakens but has a lasting effect on the low level flow field. The second kind of error which is initially very small but dominates towards the end of the forecast, is the weakening of the anti-cyclonic circulations in the north and south Atlantic. In the upper troposphere the errors in the wind field become more widespread with a general increase in the equatorial easterlies. There are indications that a better representation of cumulus friction can reduce this error in part (J-F. Geleyn, Personal Communication). As discussed in Heckley (1981), this is an error common to almost all numerical models in the tropics.

6. MEAN DIVERGENT CIRCULATIONS IN THE TROPICS

Shown in Fig. 20 are the velocity potential fields at 1000 mb for the initialized and uninitialized monthly mean analyses for March 1981. Over most of the tropics the velocity potential field has been slightly weakened by the initialization. The most noticeable difference occurs over the western Pacific, Indonesian region where there has been a weakening of the divergent circulation. Fig. 21 shows the same fields at 850 mb level. At this level the main differences again occur in the western Pacific, Indonesian region; other differences, such as a slackening of gradients over Colombia, can also be seen but are quite small.

As the initialization procedure is only effective on the first five vertical modes features with a small vertical scale in the lower troposphere should be unaffected. The velocity potential at 1000 and 850 mb is largely a product of Ekman pumping in the PBL and therefore, due to the small vertical extent of the PBL, will be largely unchanged by the initialization. The larger (vertical) scale convectively driven features will be removed by the initialization as the initialization procedure does not include physical (as opposed to dynamic) processes. Thus the changes in the velocity potential field in the western Pacific, Indonesian region are most likely due to failure of the initialization procedure to retain the observed large-scale convective circulations.

Fig. 22 shows the same fields at the 200 mb level, here the initialisation has had a dramatic effect throughout the tropics, considerably reducing the gradients. It is of some note that although the amplitude has been considerably reduced the overall pattern is left unchanged.

Fig. 23 shows the velocity potential fields at 1000 mb and 850 mb for the 24-hour forecast. At 1000 mb the divergent circulation has increased slightly in intensity and over most of the tropics is very similar to the uninitialized analyses. The divergent circulation in the western Pacific, Indonesian region removed by the initialization, has returned with almost its original magnitude although the centre is slightly too far eastward. The gradients over South America have returned to about the level of the uninitialized analyses. The largest change has occurred over Africa where the velocity potential has a value twice that of either analyses. At 850 mb the divergent circulation is generally more intense than in either analyses, especially over Africa where the velocity potential has a magnitude some three times that of the analyses.

Fig. 24 shows the velocity potential at 200 mb for the 24-hour forecast. In common with the velocity potential at 850 mb considerable intensification has occurred during the first 24 hours of the forecast. Comparing with the uninitialized analysis, the gradients are slightly too intense in the equatorial central Pacific, too weak in the equatorial western Pacific, slightly too weak in the Colombian, Venezuelan region and far too intense over central Africa, being about twice that of the uninitialized analysis.

After the first 24 hours the velocity potential over Africa weakens gradually reducing its value by $\sim$20% by day 5 at both 850 and 200 mb. The large velocity potential in the Pacific at day 1 weakens, intensifying towards the west at 850 mb, but not at 200 mb. This weakening in the central Pacific is consistent with the reduction of rainfall in this region during the first

five days of the forecast, described in section 3.

Fig. 25 shows the velocity potentials at 1000 and 200 mb at day 10 of the forecast. The 1000 mb field has all the gross features of the analyses and is nearer to the analyses in intensity than is day 1 or day 5, although it misses important details such as the trough in the central Pacific. At 200 mb the gradients are nearer the uninitialized analysis in intensity than in earlier forecasts but are badly located, particularly over the Pacific. The pattern over Africa at this time looks fairly good, considering the problems earlier in the forecast over this region.

7. FLOW VARIATIONS IN THE EARLY STAGES OF THE FORECAST

The very rapid overdevelopment of the divergent circulations during the first 24 hours of the forecasts, particularly in the region of central Africa, suggests an imbalance in the models initial state. The initialisation procedure used to filter out the high frequency gravity waves in the initial conditions has the unfortunate effect of considerably damping out the tropical divergent circulations, as has been illustrated in the velocity potential diagrams shown in the previous section. During the forecasts the model rapidly develops its divergent circulations and by 6 hours has produced vertical velocities in the tropics of realistic magnitudes. The wind field at 6 hours is still fairly close to the analyses with maximum errors of about 1 ms^{-1} at 850 mb and about 2 ms^{-1} at upper levels. These errors occurring principally in the African region and to a lesser extent off the west coast of South America. It is of interest to study the changes in the flow during the ensuing 18 hours i.e. from 6 to 24 hours.

Fig. 26 shows the monthly mean differences in the windfield between the 24 hour and 6 hour forecasts at 850 mb and 150 mb. The differences are generally slightly larger at 150 mb than 200 mb therefore the discussion will concentrate on this level. Studying these figures it is clear that there are two main problem areas, Africa and South America, the largest errors occurring over Africa. Looking in detail at these two areas we see remarkable similarity in the difference fields. At 150 mb there are strong westerlies over East Africa and the western Indian Ocean, and strong easterlies over West Africa and the eastern Atlantic. To the north and south of the easterlies are anticyclones. A similar pattern is to be found over west South America. The flow at 850 mb is in antiphase to this. This type of flow pattern observed over the African and South American regions has been reproduced in analytic models; the simplest of which is Gill's (1980) analytic model of steady heat induced tropical circulations; simple because it only describes Kelvin and Rossby waves as

as free modes. Fig. 27 shows his steady state solution for heating symmetric about the equator. The figure shows the solution at the ground. It has a cosine variation of the horizontal velocity fields and pressure perturbations with height. The solution shows inflow into the heating region near the surface and outflow at upper levels. The zone of easterlies to the east of the forcing region is more intensive than the zone of westerlies to the west because the Kelvin wave has a phase speed three times that of the gravest Rossby wave. There is a 'Walker' type of circulation in the east west and a Hadley circulation in the north south. The circulation in the Walker circulation is about five times that in each of the Hadley cells. In the heating region, $|x| < 2$, there is poleward flow in the lower layer in accordance with the vorticity equation ($\beta v = f \partial w/\partial z$). The return flow is situated farther west because it is associated with the symmetric Rossby wave which propagates that way. Gill's steady state theory has been extended to time dependent flows and similar results are obtained (Heckley and Gill, 1983).

Comparing the simple solution in Fig. 27 with the differences in Fig. 26, it is tempting to conclude that the model's vertical velocity is too large over Central Africa and the Colombian/Peruvian region. However, the problem is not so straightforward, as demonstrated by Simmons (1982, b) the static stability may also play an important role in generating these disturbances. Nevertheless, it is clear from the precipitation patterns described earlier that these patterns are originating from the most convectively active regions of the tropics. These ideas suggest that the growth of the model errors during this early stage of the forecast may be related to problems with a few particular types of wave. In order to investigate these ideas further the differences between the 24 and 6 hour forecasts were projected onto the normal modes of the model. The following discussion will concentrate on these 18 hour differences. Fig. 28 shows the relative amplitudes of the first five vertical modes for the gravity modes. Most of the amplitude is in vertical modes 3 and 4, and for the Rossby modes (not shown) in vertical mode 2. These modes have their largest amplitudes at upper levels. Fig. 29 shows the wavenumber spectrum for the gravity modes for vertical mode 3, the largest amplitude occurs in the eastward propagating gravest symmetric mode, i.e. the Kelvin wave, at zonal wavenumber 4; it is also the Kelvin wave which dominates in vertical mode 4. The westward propagating gravity waves also have a large component in the gravest meridional mode at zonal wavenumber 4. Fig. 30 shows the wavenumber spectrum for the Rossby (and mixed Rossby-Gravity) modes for vertical mode 2; these are, of course, all westward propagating. The largest amplitude occurs in the gravest meridional mode at zonal wavenumber 2, the gravest anti-symmetric mode also has large amplitude in the first vertical mode.

Fig. 31a shows the total gravity wave component of the windfield at 150 mb and Fig. 31b shows the total Rossby wave component at 150 mb, for the first five vertical modes and 20 zonal modes. Comparing with the totals in Fig. 26a it is clear that a large part, but not all, of the windfield is accounted for, and is split roughly equally between the gravity and Rossby modes. We can see from Fig. 26a that even in the monthly mean there is considerable small scale structure that would contribute at zonal wavenumber > 20. Fig. 32 shows the corresponding wind fields at 850 mb. At this level a large part of the total wind field is not accounted for by these modes, and is presumably described by the higher vertical modes not considered here.

Fig. 33 shows the velocity potential field of the total differences at 150 mb and 850 mb, and Fig. 34 shows the velocity potential field of the gravity wave component at these levels. The gravity wave component accounts for almost 100% of the velocity potential at 150 mb and a large part of the field at 850 mb. Fig. 35 shows that at 150 mb this velocity potential is split roughly equally between the Kelvin wave and the gravest symmetric westward gravity mode, with the Kelvin wave having slightly more amplitude. Fig. 36 shows that at 850 mb the velocity potential field is dominated by the Kelvin wave. Shown in Fig. 37 are the Kelvin wave (a) and the gravest symmetric westward gravity mode (b), these two modes are the largest contributors to the total gravity mode contribution. There appear to be two distinct sources for the Kelvin wave, central Africa and western South America. The westward gravest symmetric gravity mode has one principal source over Central Africa and has slightly less magnitude than the Kelvin mode in this region. Fig. 38 shows the two main contributors to the Rossby component: (b) the mixed Rossby-Gravity wave and (a) its symmetric counterpart. In agreement with Gill's (1980) simple model and Heckley and Gill (1983), the symmetric counterpart of the Rossby wave locates well with respect to the Kelvin mode shown in Fig.37a. The two Rossby modes have about the same amplitude.

The total differences at 150 mb are largely accounted by four of the gravest meridional modes: the Kelvin mode, the symmetric westward gravity mode, the mixed Rossby gravity mode and the gravest symmetric Rossby gravity mode. Each of these modes account for roughly equal amounts of the total wind, but the divergent wind is principally accounted for by the gravity modes. At 850 mb the Kelvin wave plays an important role in the total wind and the divergent wind but on its own does not go very far towards explaining the very large differences occurring at this level.

The very important role being played by the Kelvin mode in these differences has serious implications for our forecasting model. The Kelvin wave accounts for a large part of the observed energy in the atmosphere (it is presumably a quasi-stationary forced mode). The ability of our analysis scheme to treat it is under investigation. The nature of the mass wind coupling to be used in the tropics is important. The indications are that we are unable to analyse idealised Kelvin waves well with our present system because we weaken the geostrophic coupling in the tropics. A diabatic initialisation is currently under test and this could lead to a reduction in spin-up problems.

8. FLOW CHANGES AFTER THE FIRST 24 HOURS OF THE FORECAST

Fig.39(a) shows the 48-24 hr differences at 150 mb for the gravity wave component of the velocity potential; the gravity waves on this scale have very little amplitude in the streamfunction. Comparing Fig.39(a) with Fig.33(a) we see that the gravity wave changes are in the opposite sense to those occurring in the first 24 hours of the forecast. In terms of differences with respect to the analyses, the first 24 hours of the forecast is characterised by a rapid development of low level convergence and upper level divergence over the tropical continents, principally Africa. This response then appears to 'overshoot' turning to upper level convergence during the second 24 hours of the forecast. Thereafter there is little change in the gravity wave amplitudes during the forecasts. Thus the 'adjustment' of the gravity waves takes in the mean, one to two days. This time scale agrees with simple theoretical studies, e.g. Heckley and Gill (1983).

The 48-24 hr differences at 150 mb for the Rossby wave component of the streamfunction are shown in Fig.39(b). The Rossby waves on this scale have very little amplitude in the velocity potential. The changes during this period are of comparable magnitude to those during the first 24 hours of the forecast. The Rossby waves continue to change for, on average, seven to ten days into the forecast. Once again this time scale for the 'adjustment' of the Rossby waves is in agreement with the simple solutions presented in Heckley and Gill (1983).

A clear example of the problems with the planetary scale waves in the model is given by the behaviour of second internal symmetric Rossby mode. This mode is analysed to be almost stationary. The forecast (Fig.40) shows the mode to move westward at about 8° latitude per day which, again, suggests erroneous forcing.

9. CONCLUDING REMARKS

Over fairly large regions and in the monthly mean the model predicted rainfall agrees well with what limited observations are available for the first one or two days of the forecast and thereafter tends towards a reasonable agreement with climatological rainfall. The rainfall can, however, be locally very intense and, as we have seen in the experiments conducted with monsoon forecasts, this can lead to erroneous circulations developing which may be easily explained in terms of simple theoretical ideas. It is tempting also to invoke the same arguments to explain some of the very large changes that occur in the monthly mean during the forecast over the African and South American regions. Certainly we can conclude from the normal mode analysis here and the theoretical studies of Gill (1980), Heckley and Gill (1983) and Simmons (1982,b) that these circulations can be caused by erroneous vertical velocities, which suggests erroneous forcing.

These errors may be partly a result of poor analysis, partly a result of the model having to rapidly develop its own divergent circulations after they have been weakened by the initialisation and partly caused by deficiencies internal to the model. It is only possible to speculate at this stage what the causes are. The model's initial data set had until recently been adiabatically initialised. On starting a forecast with full, diabatic, physics, the flow field was no longer in balance with the forcing and the flow field began to adjust to the model's forcing, the so-called 'spin-up' process. One may expect similar problems due to an absence of a diurnal cycle of radiation in the model since there is a large diurnal cycle in observed temperatures over tropical continents. The insertion of high surface temperatures at 12Z over Africa, for example, into a relatively cool model atmosphere is very much like switching on a heat source. These are largely tropical problems as diabatic forcing is dominant in the tropics and these large scale modes have their largest amplitude in the tropics. The errors in these large scale waves account for some thirty to fifty per cent of the total errors in the tropics. However certain important aspects of the tropical circulation are maintained reasonably well, for example the trade winds at 1000 mb.

Acknowledgments

Contributions to the work presented here were made by many staff members of ECMWF, to whom gratitude is expressed.

REFERENCES

Arakawa, A. 1966 Computational design for long-term numerical integration of the equations of fluid motion: two dimensional incompressible flow. Part 1. J. Comp. Phys., 1, 119-143.

Arakawa, A. and V.R. Lamb 1977 Computational design of the basic dynamical processes of the UCLA general circulation model. Methods in Computational Physics. Vol. 17, J. Chang, Ed., Academic Press, 337 pp.

Burridge, D.M. 1979 Some aspects of large scale numerical modelling of the atmosphere. Proceedings of the ECMWF Seminar on Dynamical Meteorology and Numerical Weather Prediction. Vol. 2, 1-78.

Burridge, D.M. and J. Haseler 1977 A model for medium range weather forecasting - Adiabatic formulation. ECMWF Tech. Rep. No. 4. 46 pp.

Gilchrist, A. 1977 The simulation of the Asian summer monsoon by general circulation models. Pure and Applied Geophysics, 115, 1431-1448.

Gilchrist, A., P.R. Rowntree and D.B. Shaw 1982 Large scale numerical modelling. GARP publication series No. 25, The GARP Atlantic tropical experiment (GATE), WMO, 183-218.

Gill, A.E. 1980 Some simple solutions for heat-induced tropical circulations. Quart. J. Roy. Met. Soc., 106, 447-462.

Heckley, W.A. 1981 A survey of the performance of GCM's in the tropics - Part I: Other models. ECMWF Technical Memorandum No. 45. 26 pp.

Heckley, W.A. and A.E. Gill 1983 Some simple analytical solutions to the problem of forced equatorial long waves. Submitted to Quart. J. Roy. Met. Soc.

Jaeger, L. 1976 Monatskarten des niederschlags für die Ganze Erde. Berichte des Deutschen Wetterdienstes. Nr. 139 (Band 18).

Lorenc, A.C. 1981 A global three-dimensional multivariate statistical interpolation scheme. Mon. Wea. Rev., 109, 701-721.

NOAA 1981 Earth-Atmosphere Radiation Budget Analyses derived from NOAA Satellite Data. NOAA National Environment Satellite Service, Washington, DC, U.S.A.

Rowntree, P.R. 1978 Numerical prediction and simulation of the tropical atmosphere. Meteorology over the tropical oceans. pp. 219-249. Edited by D.B. Shaw. Published by R. Met. Soc., Bracknell.

Sadourny, R. 1975 The dynamics of finite difference models of the shallow water equations. J. Atmos. Sci., 32, 680-689.

Simmons, A.J. 1982a The numerical prediction and simulation of the tropical atmosphere - a sample of results from operational forecasting and extended integrations at ECMWF. "Tropical Droughts: Meteorological aspects and implications for Agriculture" Rf. R.P.Pearce, WMO, Geneva,81-103

Simmons, A.J. 1982b The forcing of stationary wave motion by tropical diabatic heating. Quart. J. Roy. Met. Soc., 108. In Press.

Temperton, C. and D.L. Williamson 1981 Normal mode initialization for a multi-level grid point model. Part I: Linear aspects. Mon. Wea. Rev., 109, 729-743.

Tiedtke, M., J-F. Geleyn, A. Hollingsworth and J-F. Louis 1979 ECMWF model-parameterization of sub-grid scale processes. ECMWF Technical Report No. 10, 46 pp.

Williamson, D.L. and C. Temperton 1981 Normal mode initialization for a multi-level grid point model. Part II: Non-linear aspects. Mon. Wea. Rev., 109, 744-751.

ECMWF - GLOBAL FORECASTING SYSTEM, 15-level grid point model

(Horizontal Resolution 1.875° Lat/Lon)

ANALYSIS	PREDICTION
ϕ,u,v,q(for p≥300)	T,u,v,q
p(mb)	σ
10	0.025(σ_1)
20	0.077
30	0.132
50	0.193
70	0.260
100	0.334
150	0.415
200	0.500
250	0.589
300	0.678
400	0.765
500	0.845
700	0.914
850	0.967
1000	0.996(σ_{15})

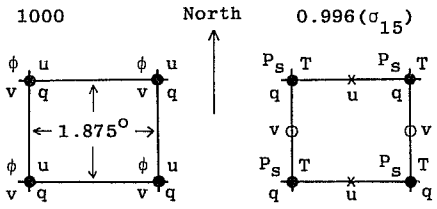

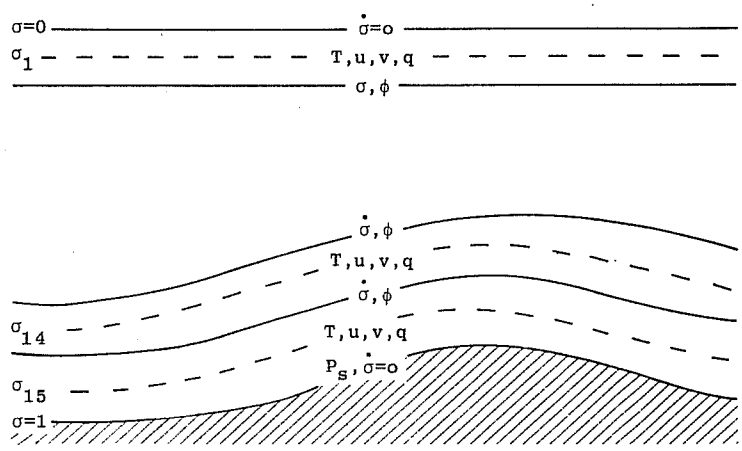

Vertical and horizontal (latitude-longitude) grids and dispositions of variables in the analysis (left) and prediction (right) coordinate systems.

ANALYSIS

Method	3 dimensional multi-variate, correction method for q
Independent variables	λ, φ, p, t
Dependent variables	ϕ, u, v, q
Grid	Non-staggered, standard pressure levels
First guess	6 hour forecast (complete prediction model)
Data assimilation frequency	6 hour ($\pm$ 3 hour window)

INITIALISATION

Method	Non-linear normal mode, 5 vertical modes, adiabatic

PREDICTION

Independent variables	λ, φ, σ, t
Dependent variables	T, u, v, q, p_s
Grid	Staggered in the horizontal (Arakawa C-grid). Uniform horizontal (regular lat/long; $\Delta\lambda=\Delta\theta=1.875^\circ$). Non-uniform vertical spacing of levels (see above).
Finite difference scheme	Second order accuracy
Time-integration	Leapfrog, semi-implicit (Δt = 15 min) (time filter ν = 0.05)
Horizontal diffusion	Linear, fourth order (diffusion coefficient = $4.5 \cdot 10^{15} m^4 s^{-1}$)
Earth surface	Albedo, roughness, soil moisture, snow and ice specified geographically. Albedo, soil moisture and snow time dependent.
Orography	Averaged from high resolution (10') data set
Physical parameterisation	(i) Boundary eddy fluxes dependent on roughness length and local stability (Monin-Obukov)
	(ii) Free-atmosphere turbulent fluxes dependent on mixing length and Richardson number
	(iii) Kuo convection scheme
	(iv) Full interaction between radiation and clouds
	(v) Full hydrological cycle
	(vi) Computed land temperature, no diurnal cycle
	(vii) Climatological sea-surface temperature

Fig. 1 The ECMWF Global Forecasting System as on 1 August 1981.

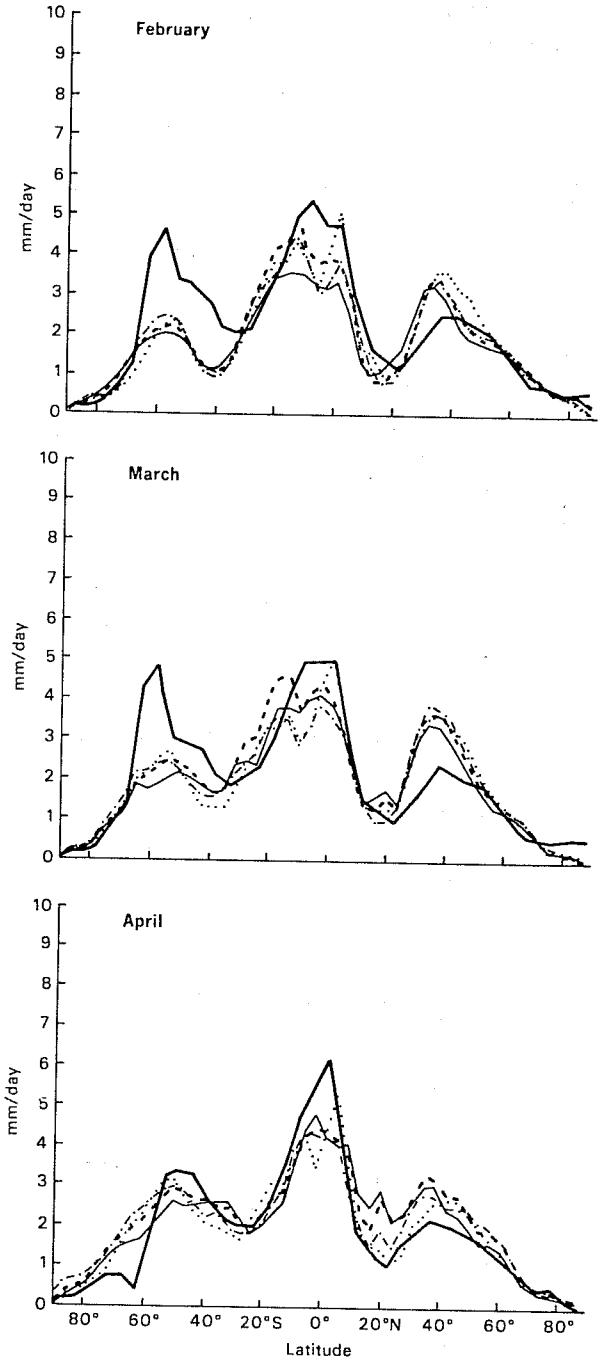

Fig. 2 Zonal mean, monthly mean forecast rainfall for the months of February, March and April 1981. The heavy solid line is the climatic value (Jaeger, 1976), the thin solid line is the 0 to 24 hour forecast rainfall, the dashed line is the 24 to 48 hour forecast rainfall, the dashed-dotted line the 96 to 120 hour forecast rainfall and the dotted line the 236 to 240 hour forecast rainfall. The units are mm per day.

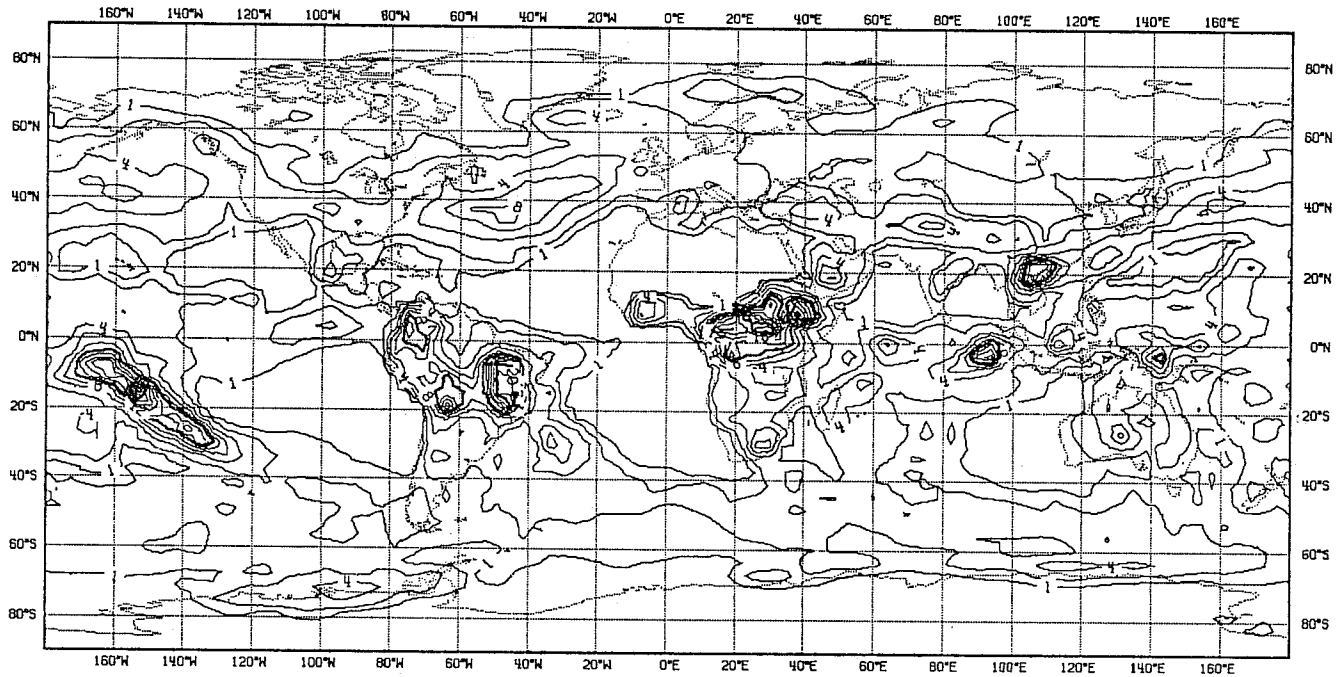

Fig. 3 Monthly mean 0 to 24 hour accumulated forecast rainfall for March 1981.
Units: mm

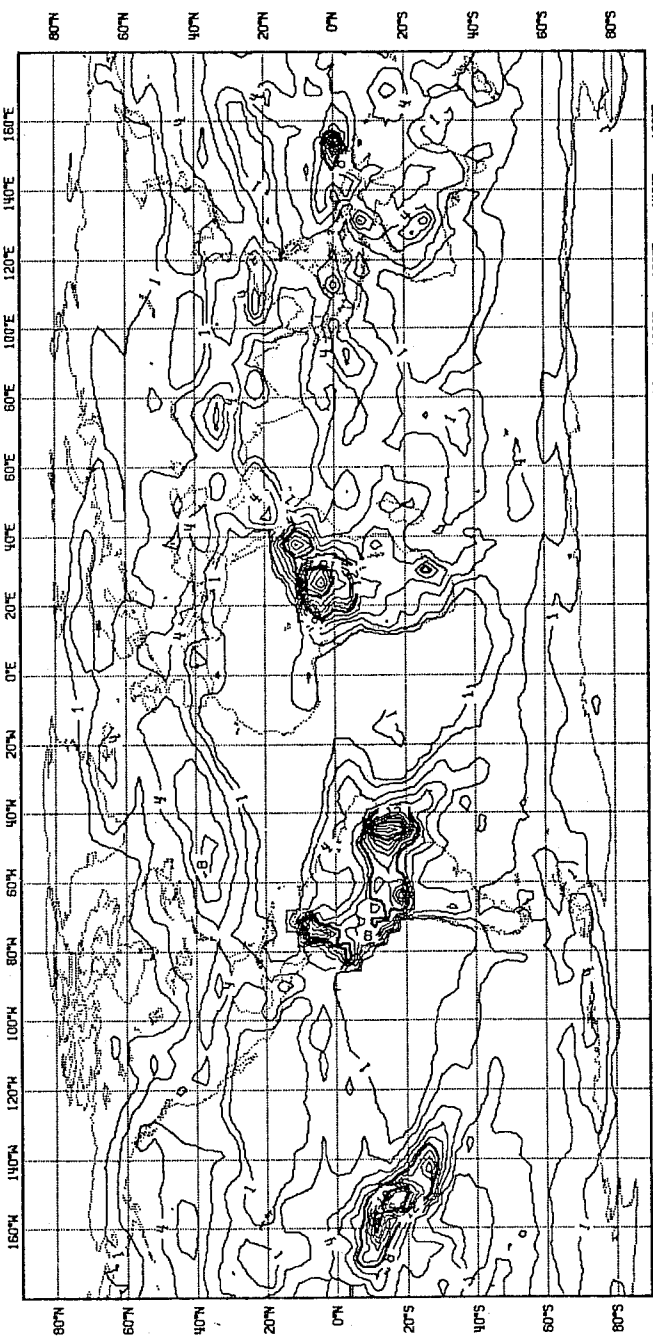

Fig. 4 As Fig. 3 for 24 to 48 hours

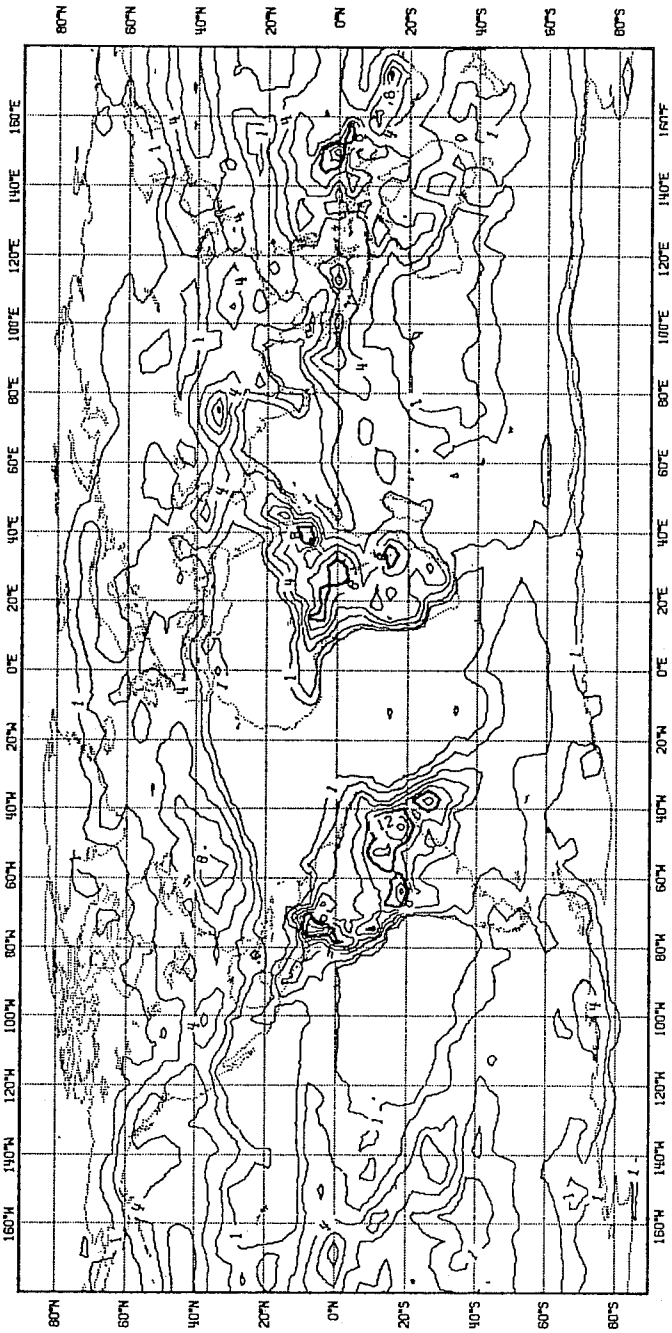

Fig. 5 As Fig. 3 for 96 to 120 hours

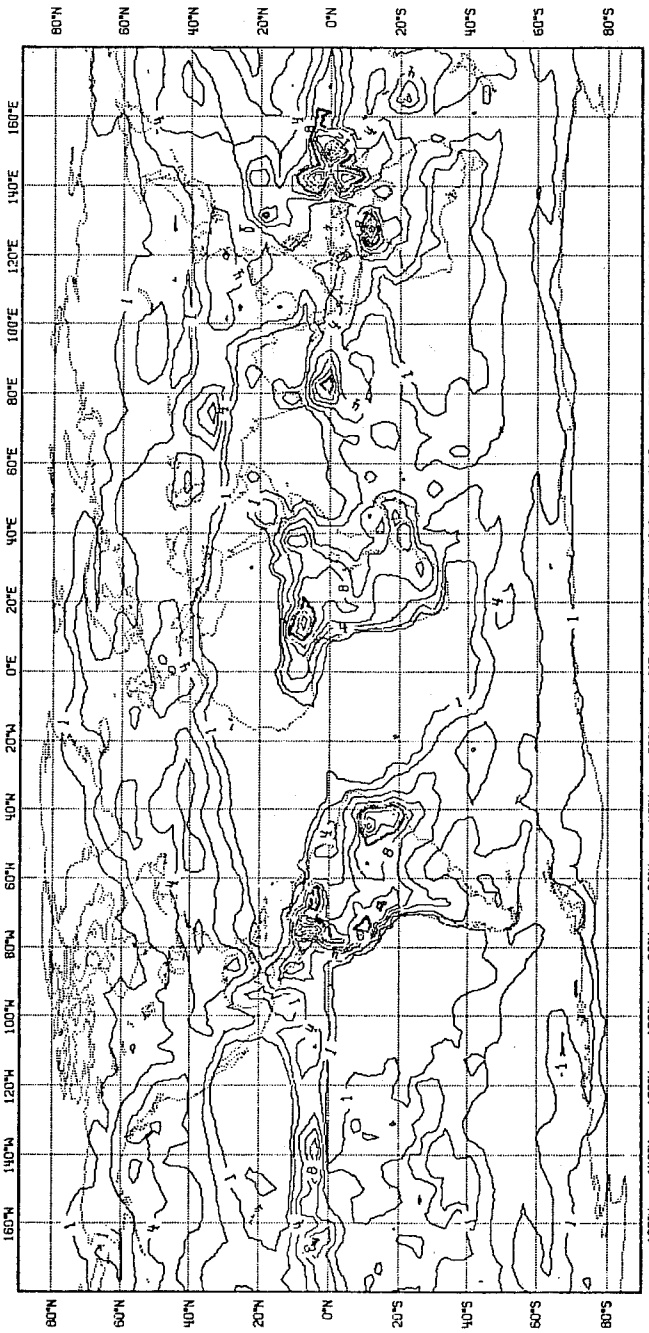

Fig. 6 As Fig. 3 for 216 to 240 hours

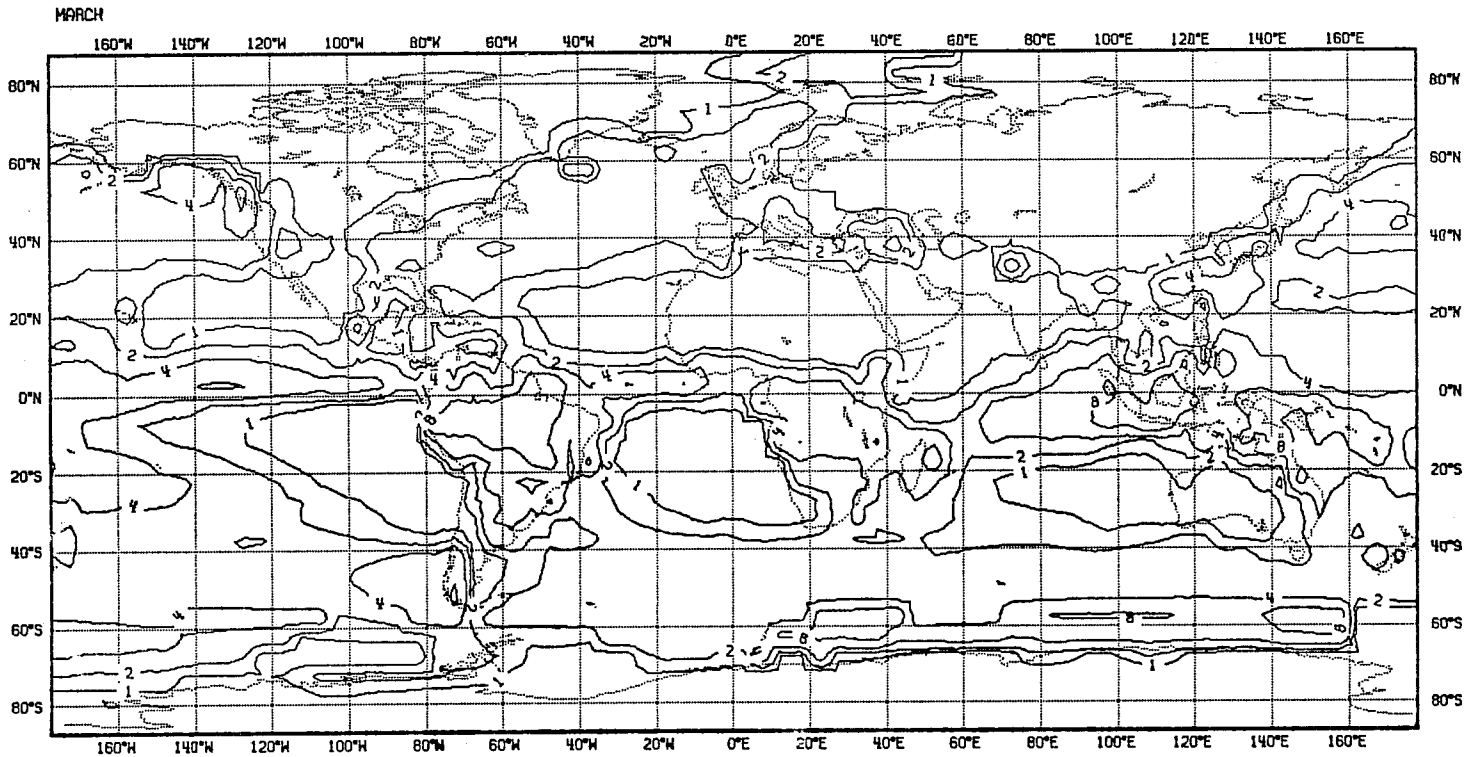

Fig. 7 Climatic distribution of rainfall for March 1981. Taken from Jaeger, 1976. The units are mm.

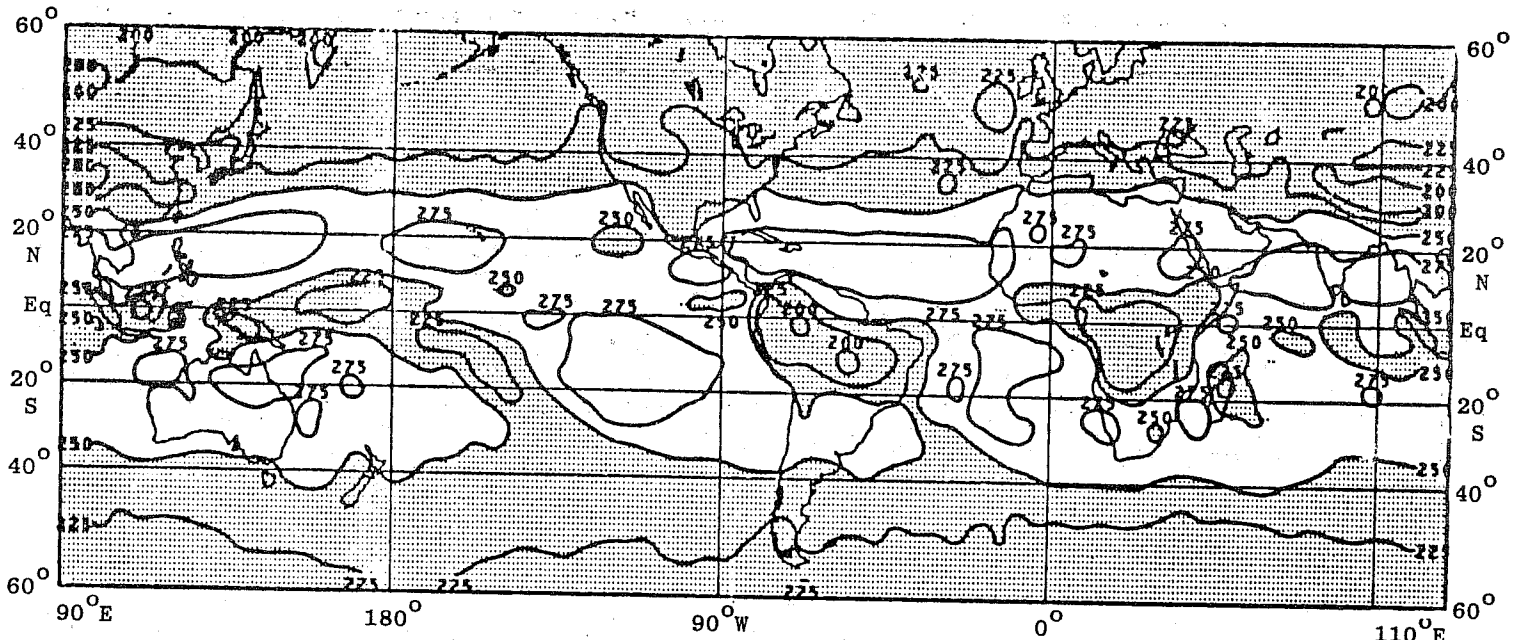

Fig. 8 The monthly mean outgoing longwave radiation for March 1981. Supplied by NOAA. The units are WM^{-2}.

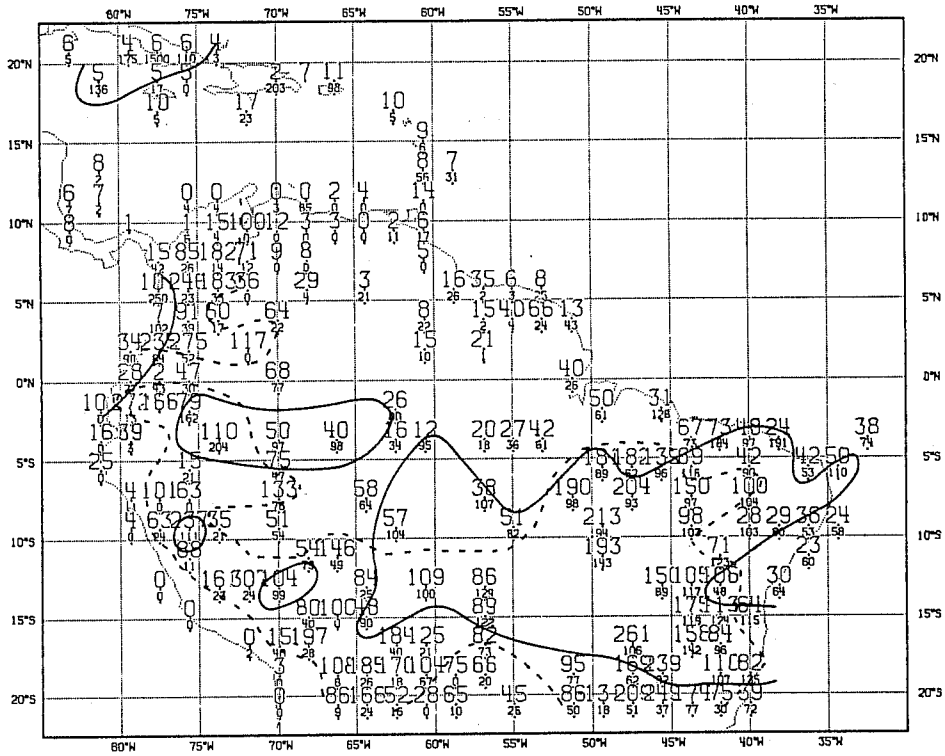

Fig. 9 Monthly average forecast and observed precipitation for March 1981. The large numbers refer to the forecast precipitation and the small numbers to the observed. The 8 mm/day contour is drawn as a solid line for the forecast and as a dashed line for the observations. The units are tenths of mm/day.

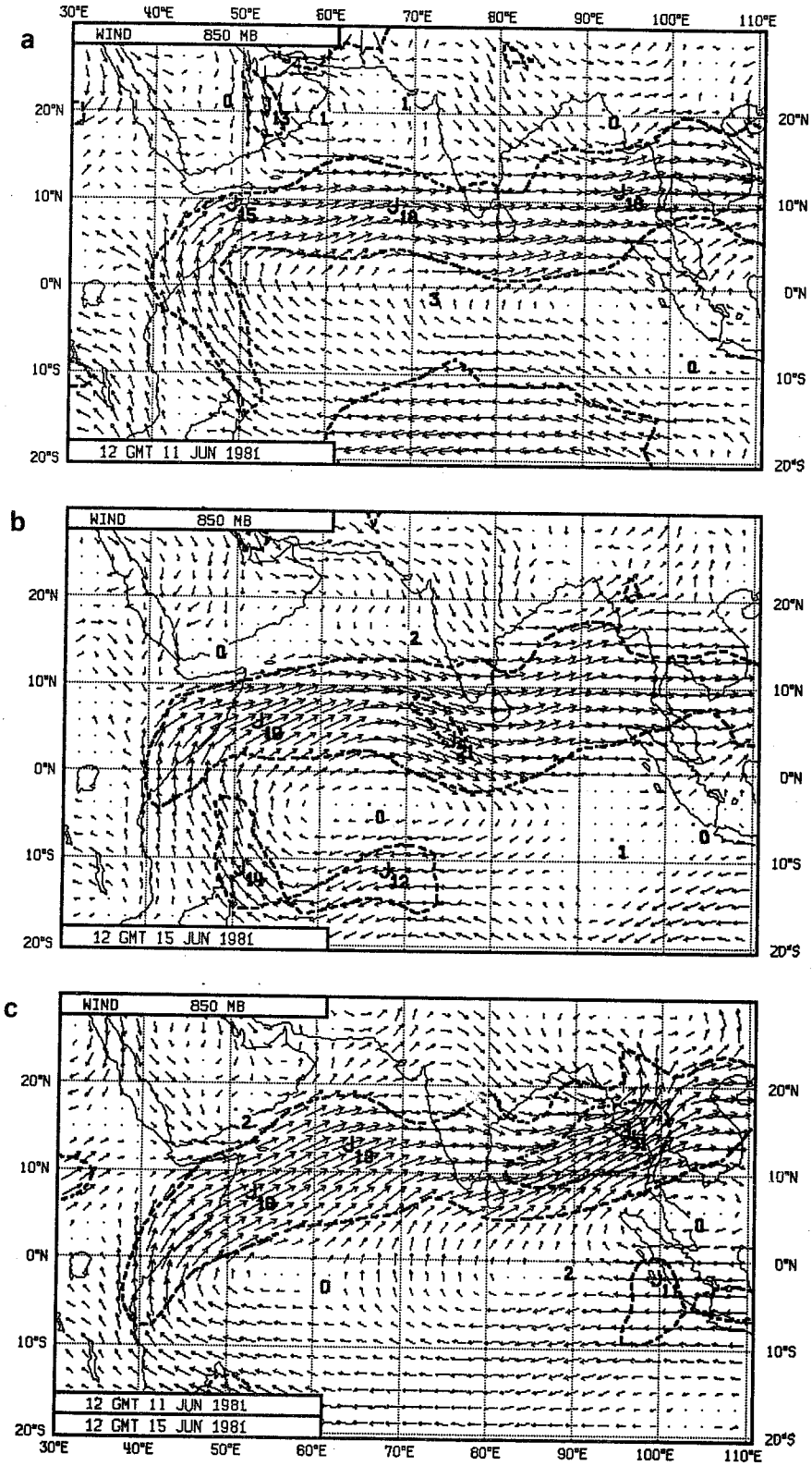

Fig. 10 Analyses of 850 mb wind for a) 11 June 1981 and b) 15 June 1981. Map c) shows the 4-day forecast from 11 June.

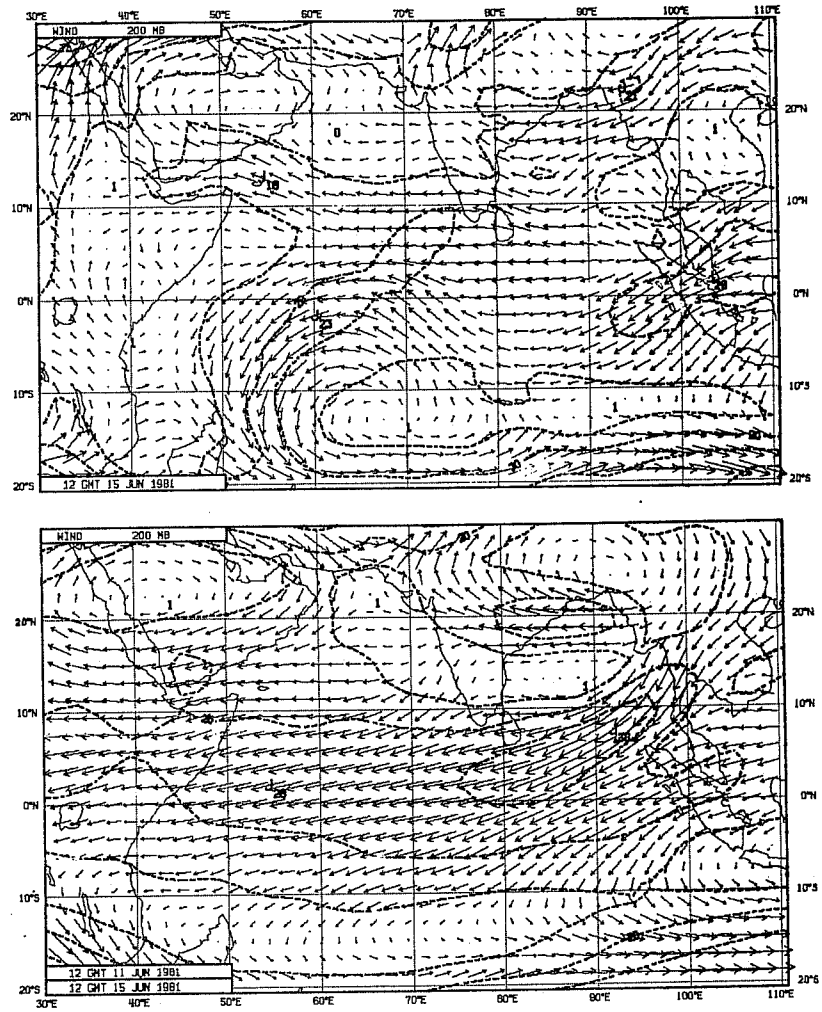

Fig. 11 200 mb wind analyses for 15 June 1981 (upper) and the corresponding 4-day forecast verifying on this date.

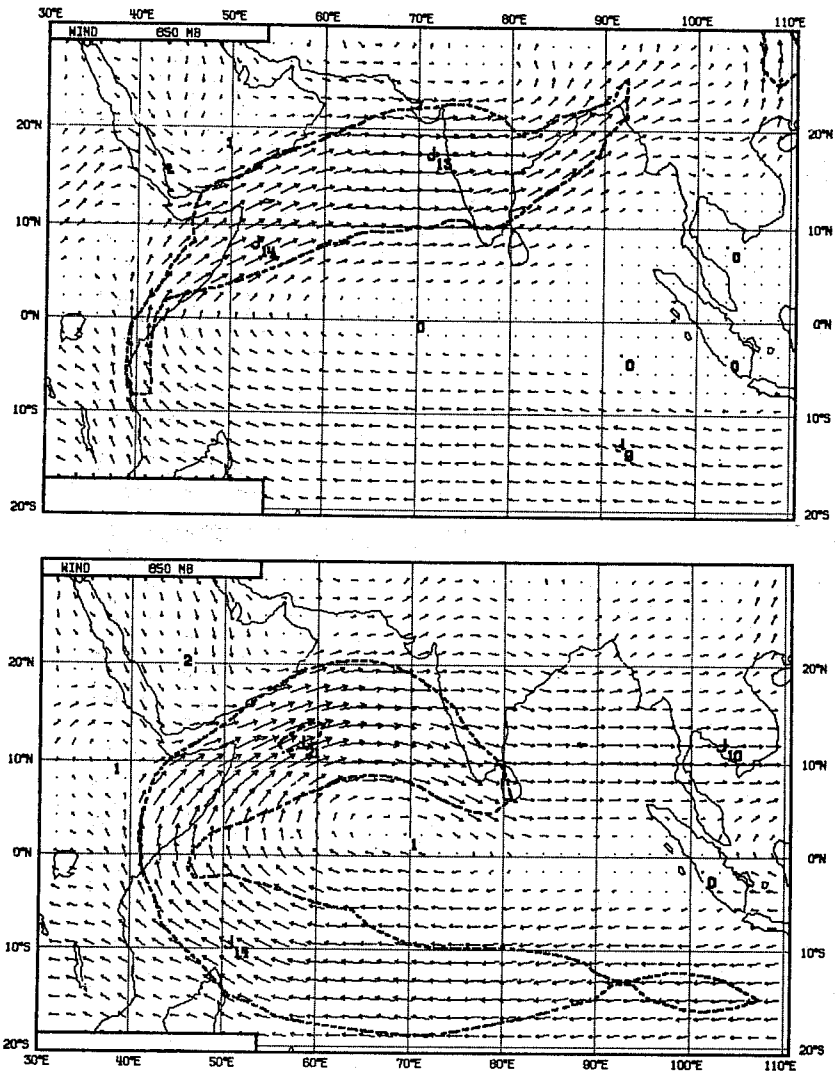

Fig. 12 Mean 850 mb wind from the last 30 days of the 50-day integration from 11 June (upper). The corresponding FGGE analysis is shown in the lower map.

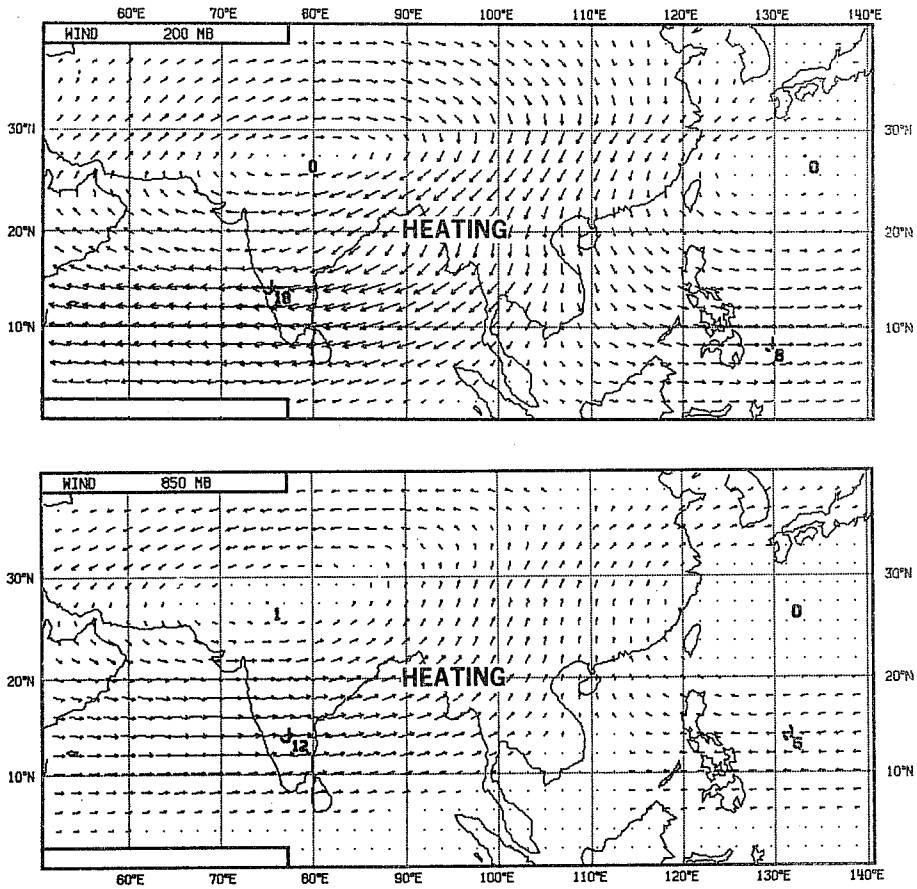

Fig. 13 300 mb (upper) and 850 mb (lower) perturbation wind fields forced in a linear, steady-state primitive-equation model by a localised heating. A July zonal mean basic state is used in the calculations.

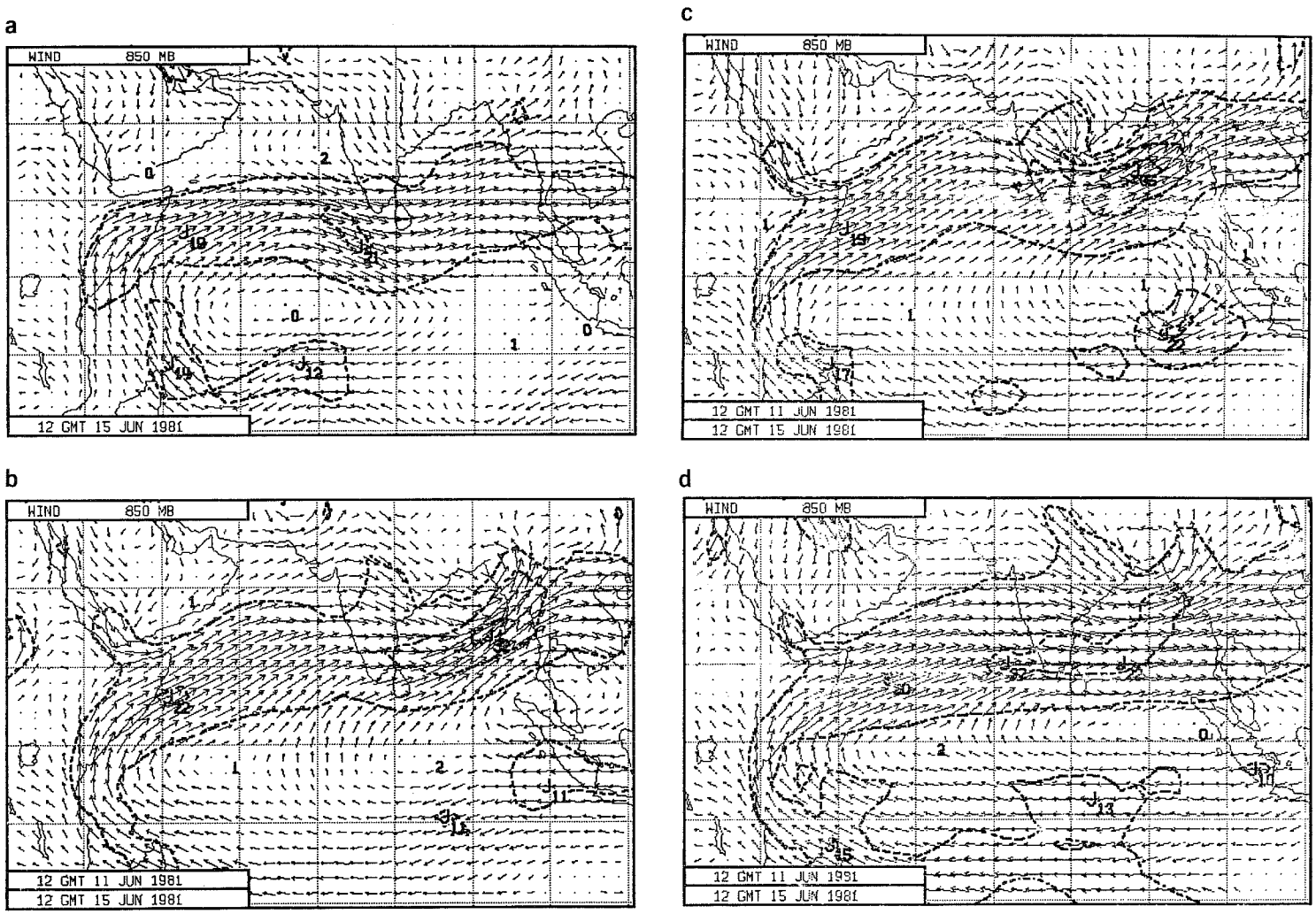

Fig. 14 a) 850 mb wind analysis for 15 June 1981 and 4-day forecasts verifying on this date using b) the Kuo convection scheme, c) moist-adiabatic adjustment and d) the Arakawa-Schubert convection scheme.

OPERATIONAL ANALYSIS

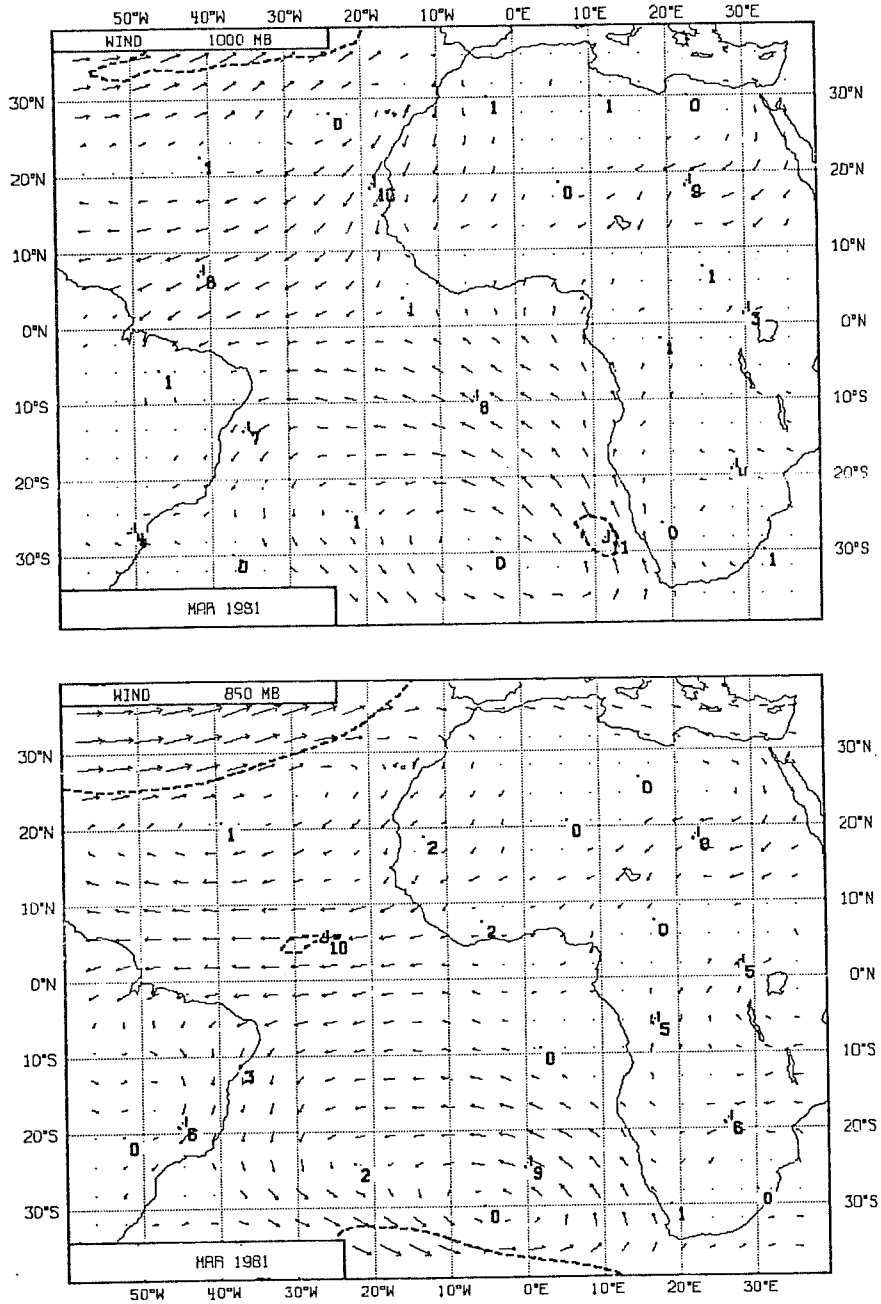

Fig. 15 The wind vectors over the Atlantic region corresponding to the operational analysis for the monthly mean for March 1981. Local maxima are indicated by numbers and the units are ms^{-1}.

Top: 1000 mb Bottom: 850 mb

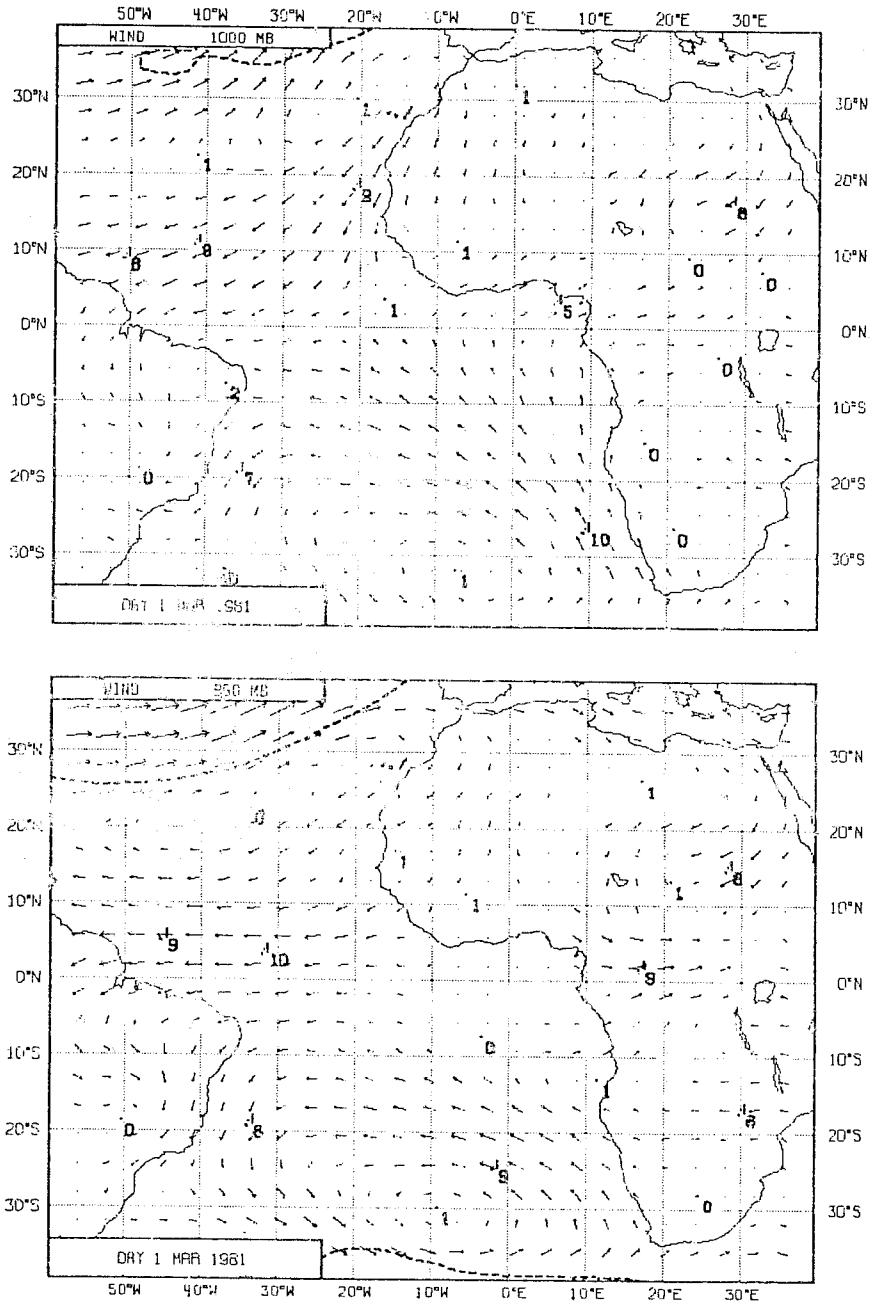

Fig. 16 As Fig. 15 for the 24 hour forecast.

OPERATIONAL FORECAST

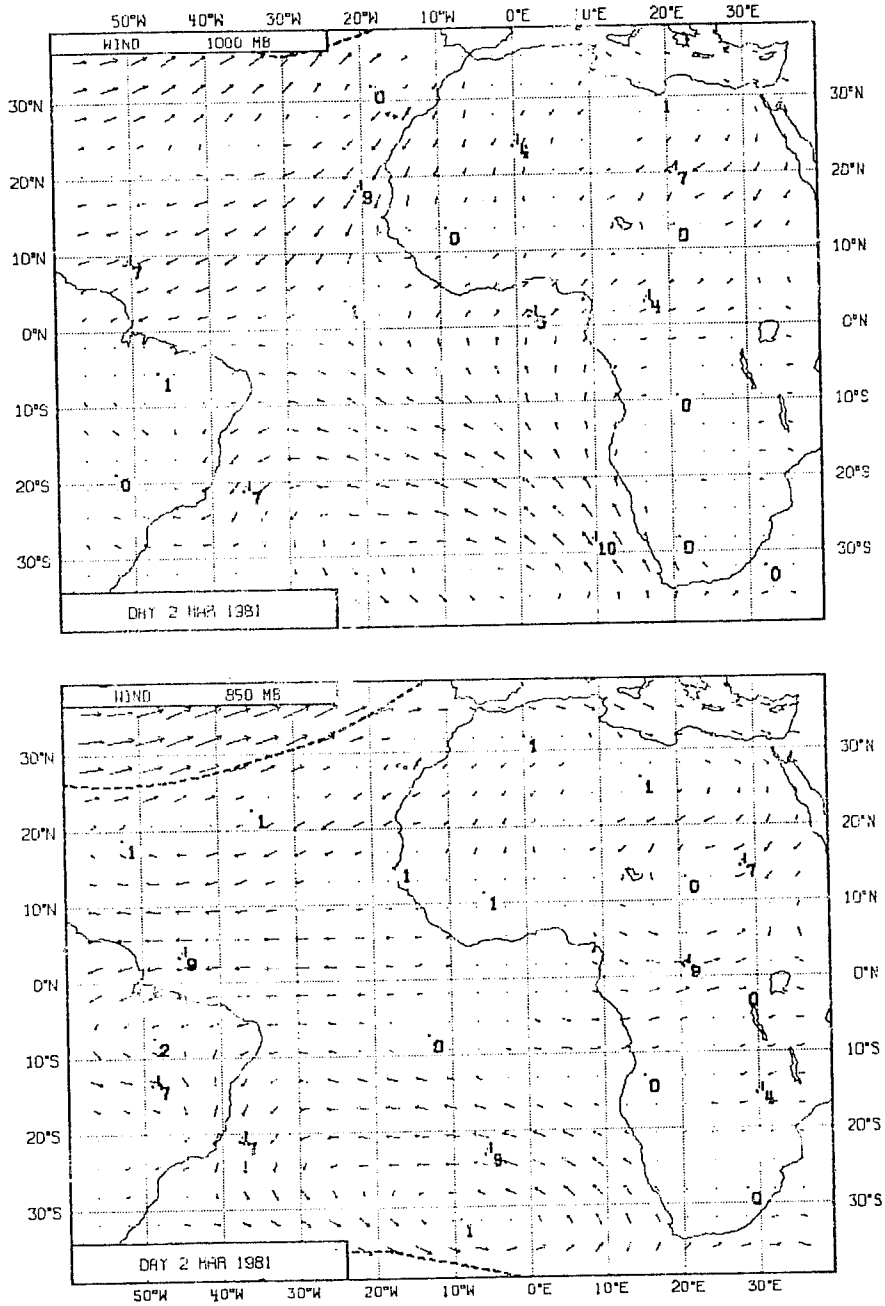

Fig. 17 As Fig. 15 for the 48 hour forecast.

OPERATIONAL FORECAST

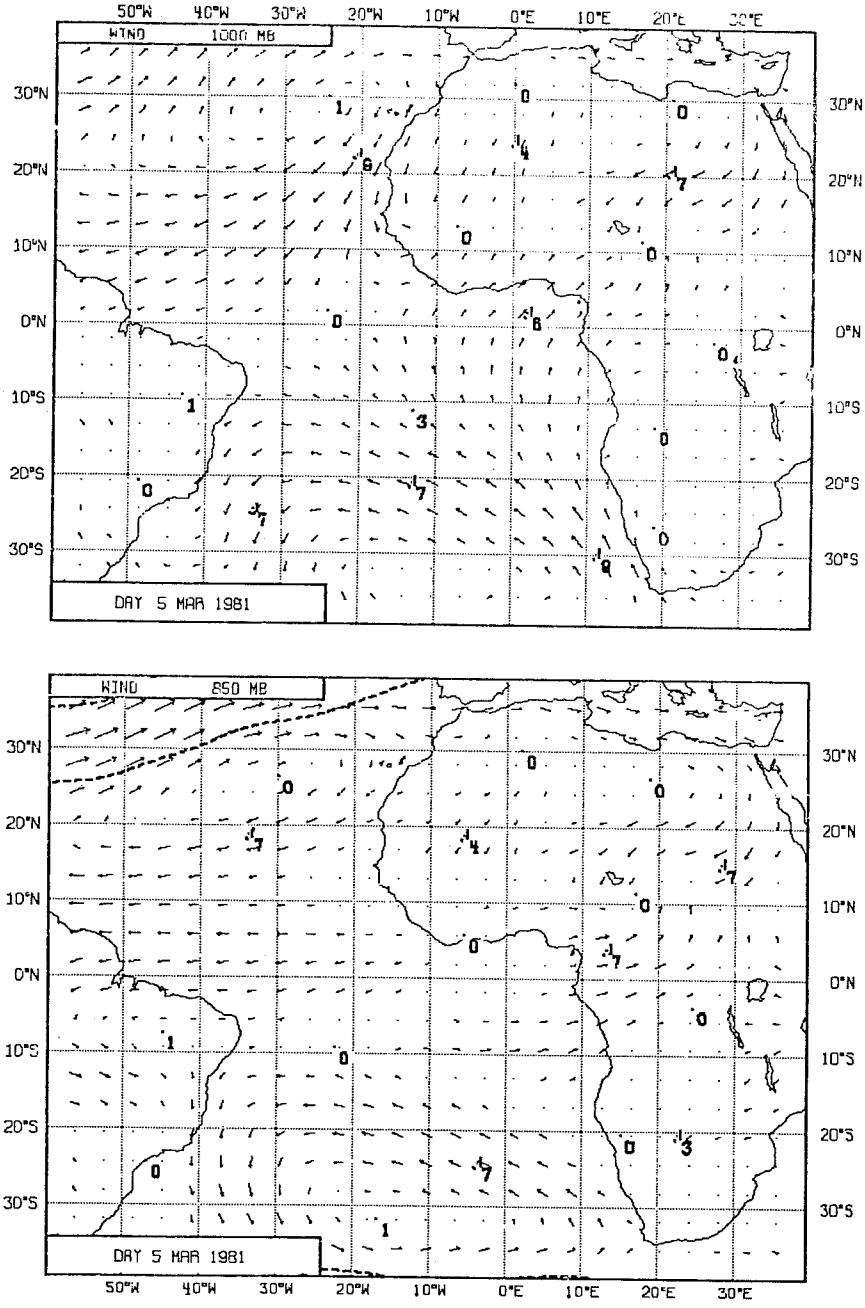

Fig. 18 As Fig. 15 for the 120 hour forecast.

OPERATIONAL FORECAST

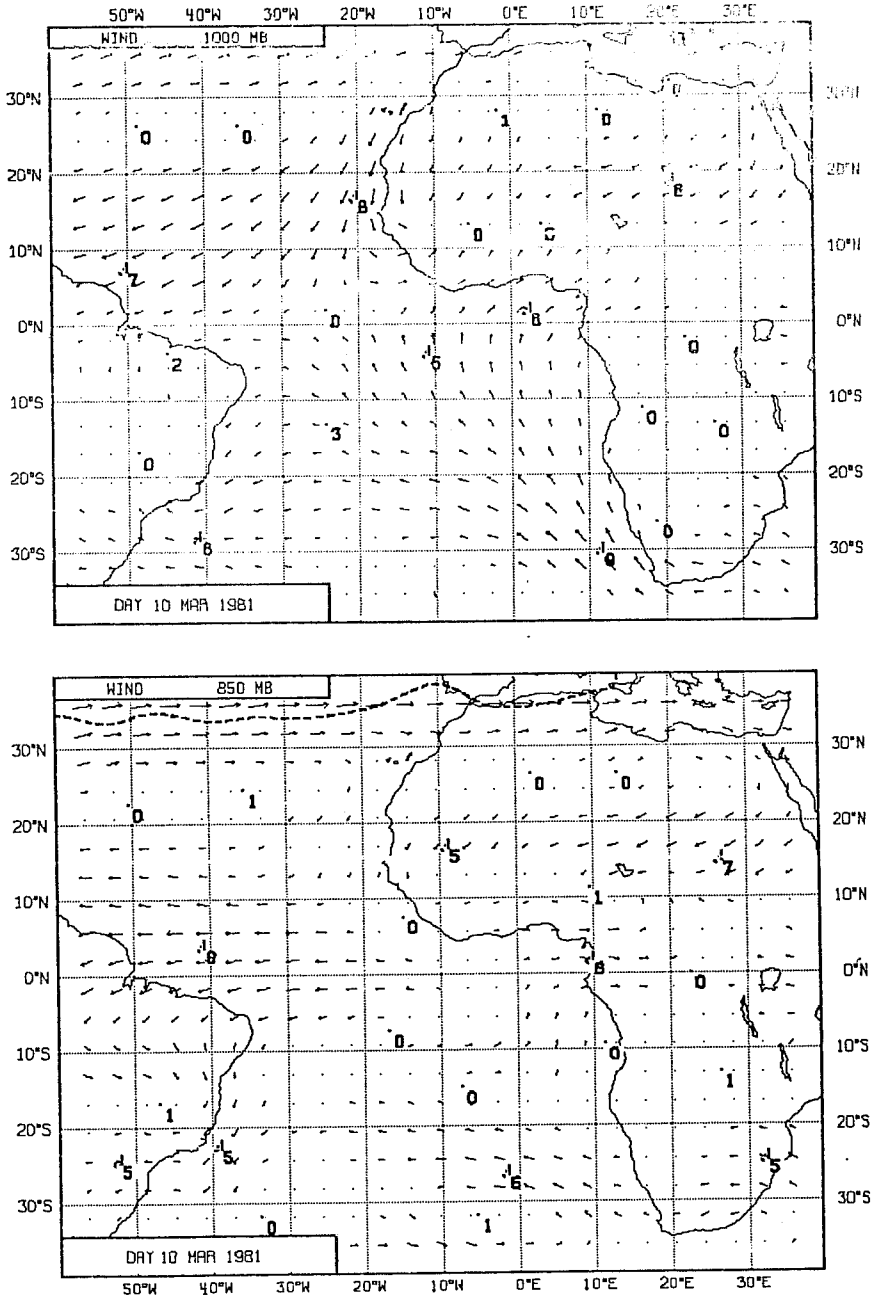

Fig. 19 As Fig. 15 for the 240 hour forecast.

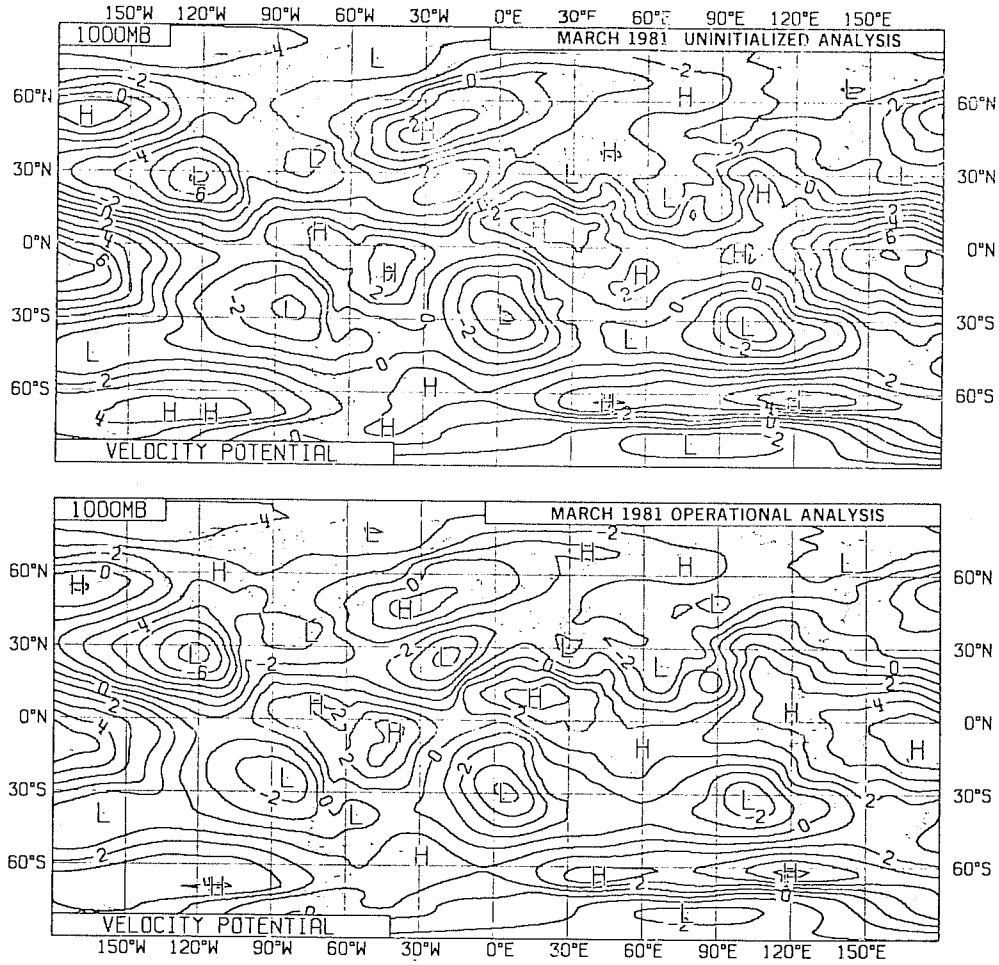

Fig. 20 Monthly mean velocity potential fields for March 1981 at 1000 mb

Top: The uninitialized analysis.

Bottom: The initialized analysis. The units are $10^{-6} m^2 s^{-1}$.

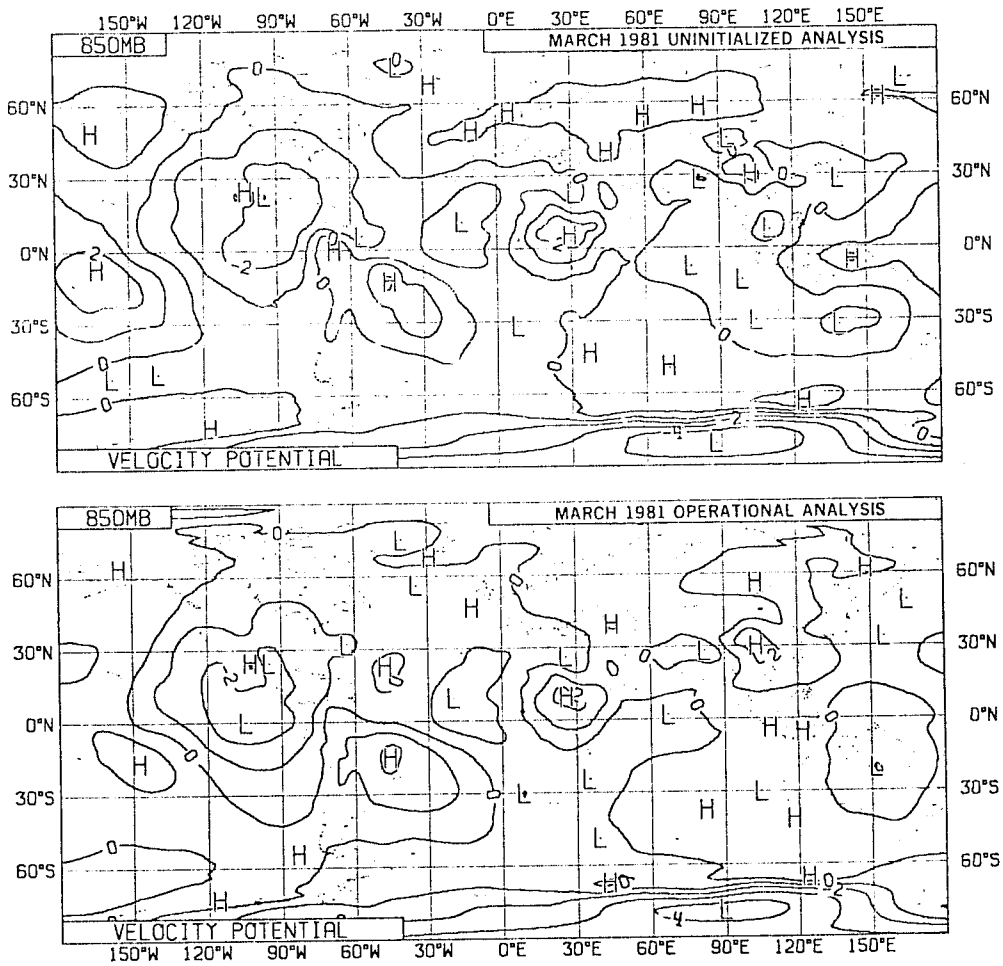

Fig. 21 As Fig. 20 but for 850 mb.

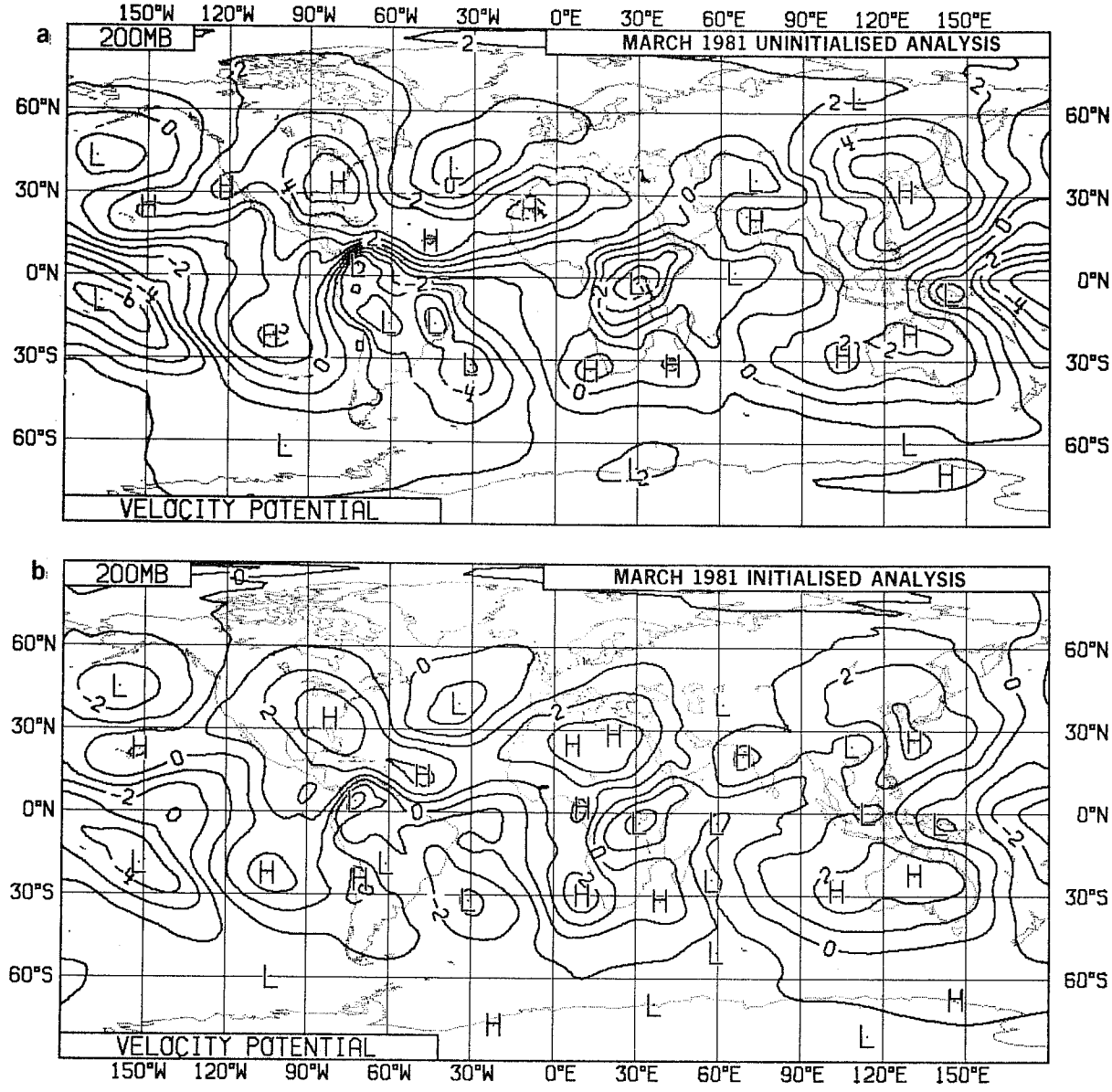

Fig. 22 As Fig. 20 but for 200 mb.

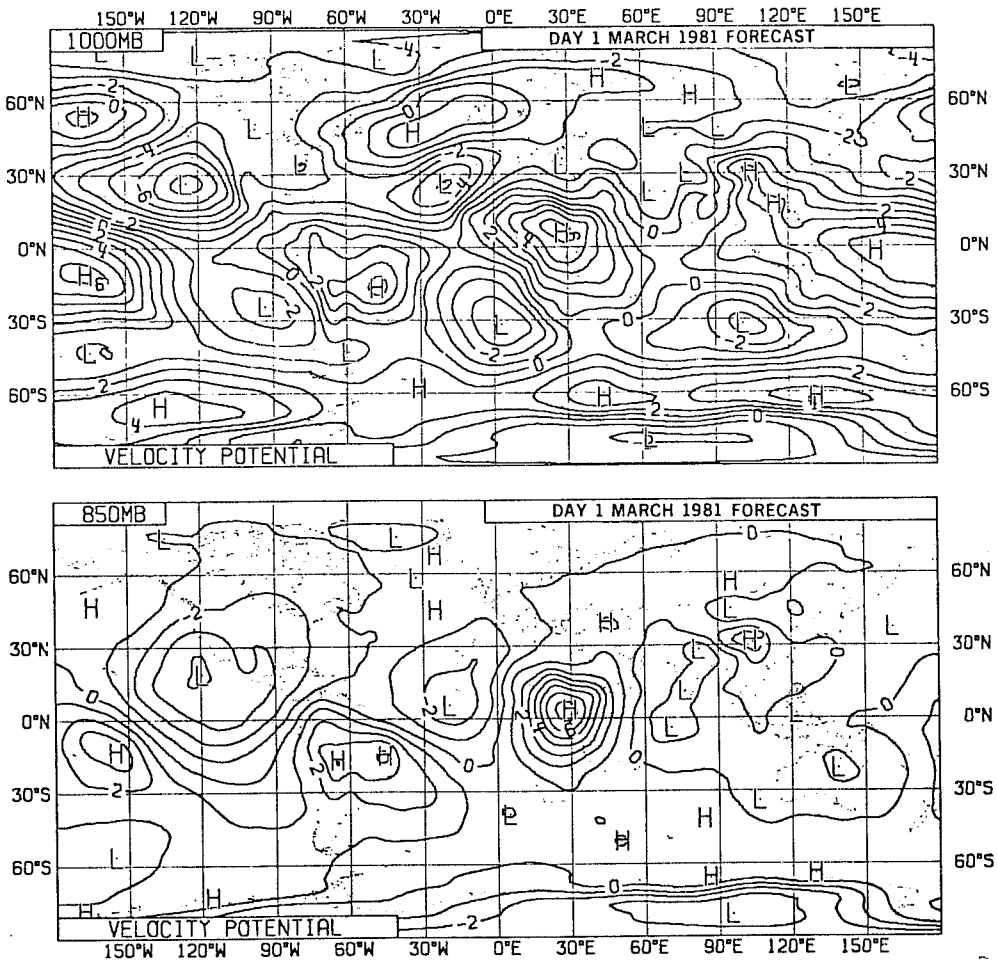

Fig. 23 Monthly mean velocity potential fields for the 24 forecast for March 1981

Top: 1000 mb

Bottom: 850 mb. The units are 10^{-6} m^2 s^{-1}.

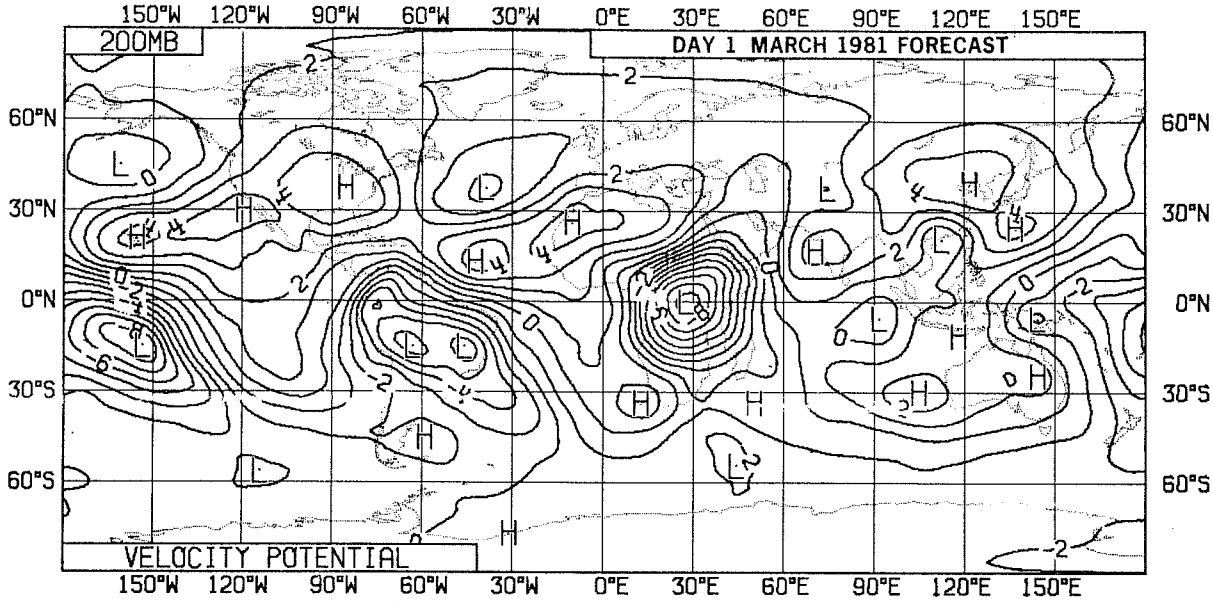

Fig. 24 As Fig. 23 but for 200 mb.

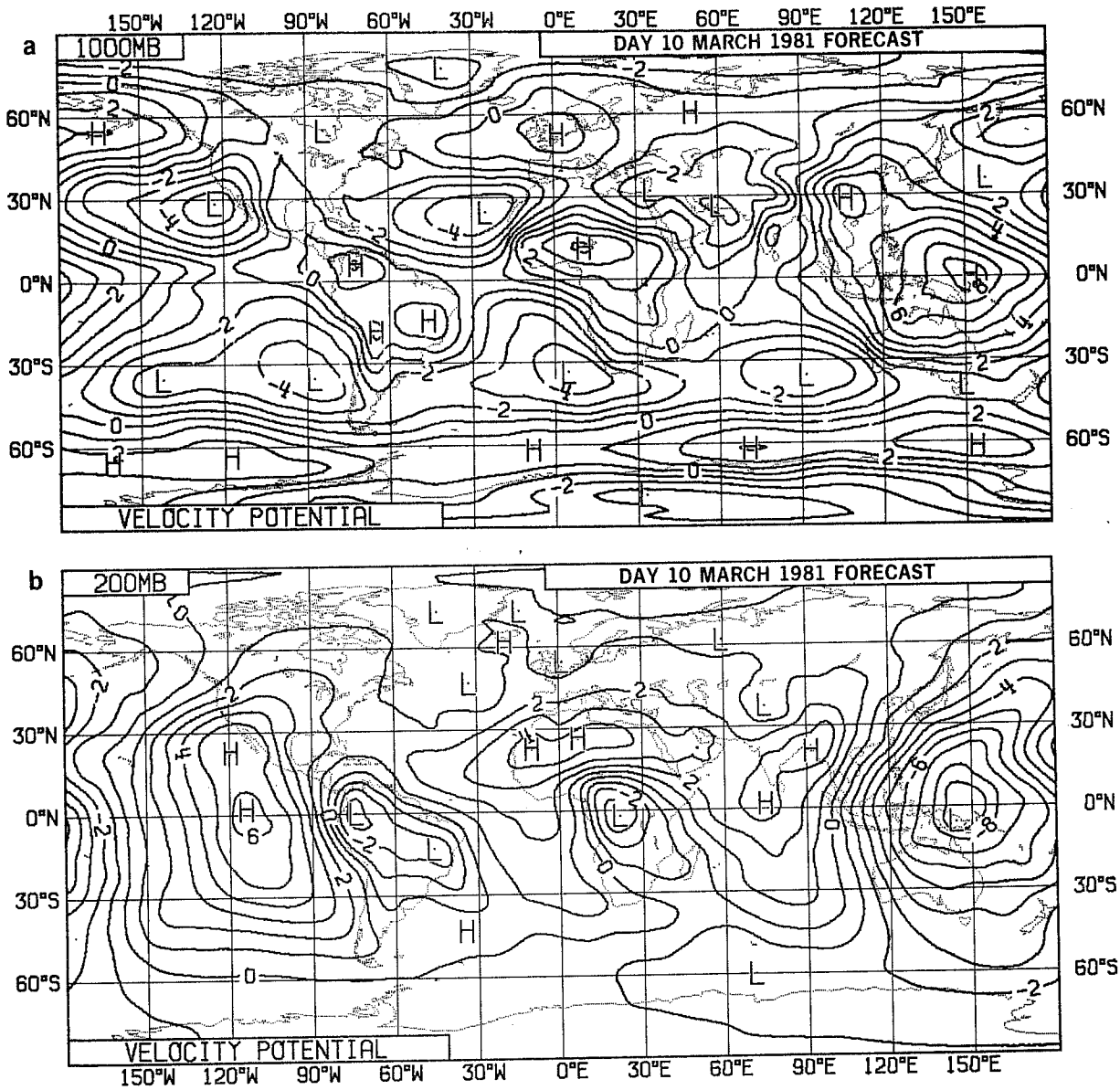

Fig. 25 As Fig. 23 but for the 24 hour forecast at 1000 mb and 200 mb.

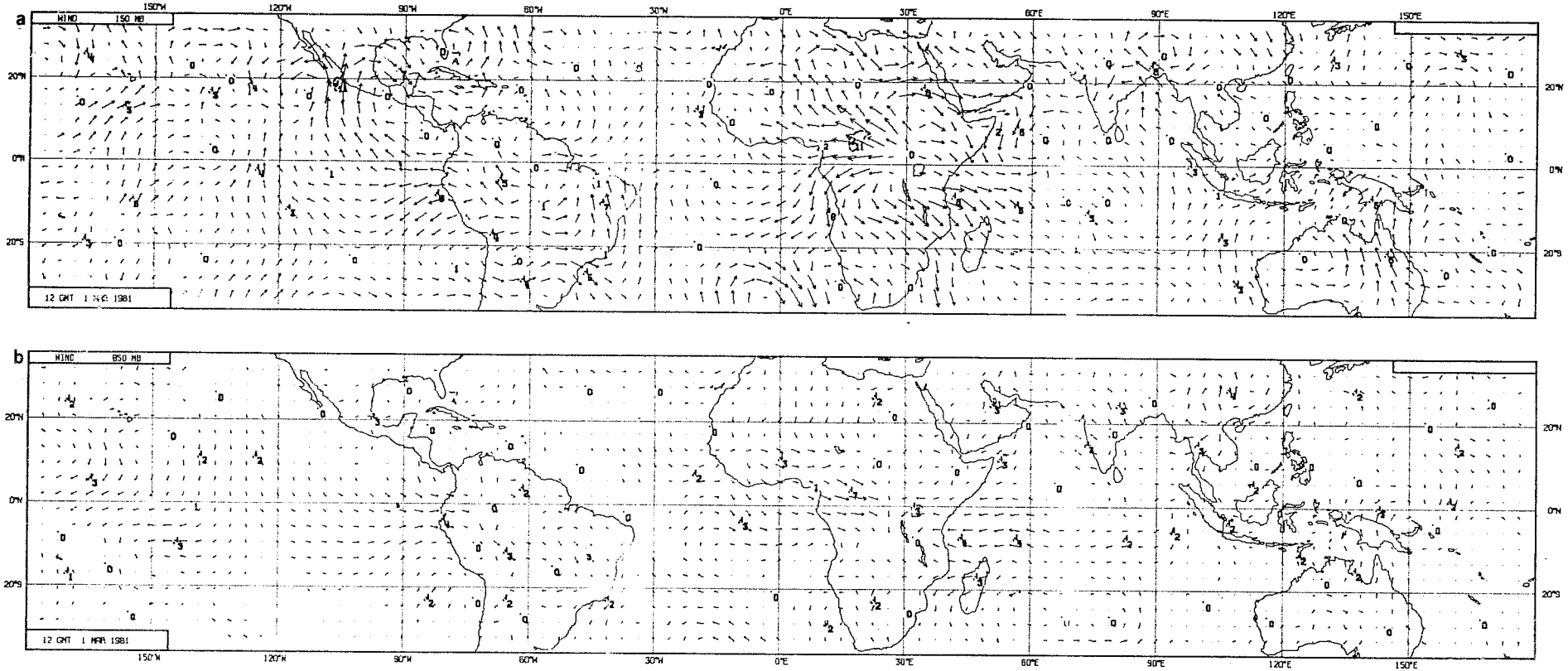

Fig. 26 Vector wind difference between March mean 24 hour forecast and the March mean 6 hour forecast for 1981. a) 150 mb, b) 850 mb.

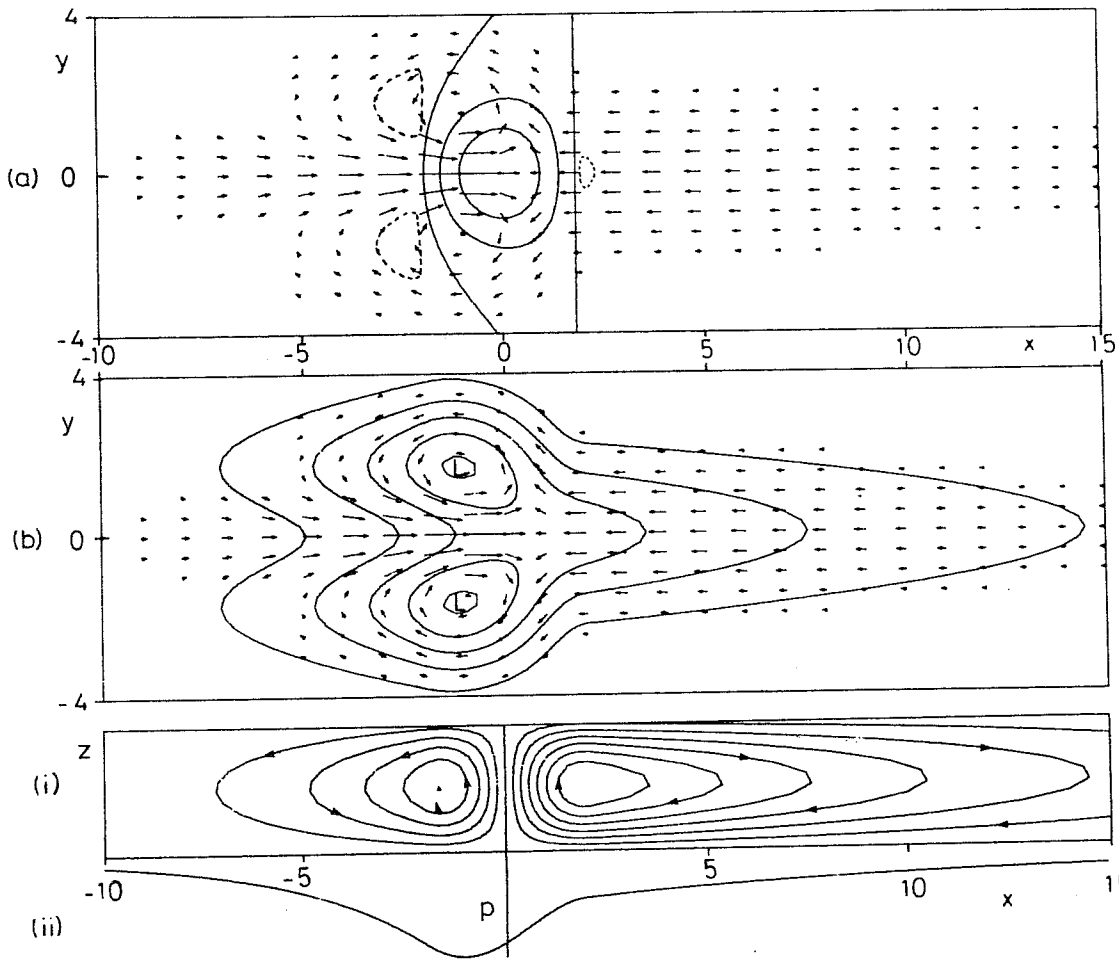

Figure 1. Solution for heating symmetric about the equator in the region $|x| < 2$ for decay factor $\varepsilon = 0{\cdot}1$

(a) Contours of vertical velocity w (solid contours are 0, 0·3, 0·6, broken contour is $-0{\cdot}1$) superimposed on the velocity field for the lower layer. The field is dominated by the upward motion in the heating region where it has approximately the same shape as the heating function. Elsewhere there is subsidence with the same pattern as the pressure field.

(b) Contours of perturbation pressure p (contour interval 0·3) which is everywhere negative. There is a trough at the equator in the easterly régime to the east of the forcing region. On the other hand, the pressure in the westerlies to the west of the forcing region, though depressed, is high relative to its value off the equator. Two cyclones are found on the north-west and south-west flanks of the forcing region.

(c) The meridionally integrated flow showing (i) stream function contours, and (ii) perturbation pressure. Note the rising motion in the heating region (where there is a trough) and subsidence elsewhere. The circulation in the right-hand (Walker) cell is five times that in each of the Hadley cells shown in (c).

Fig. 27 Gill's (1980) steady state solution for heating symmetric about the equator.

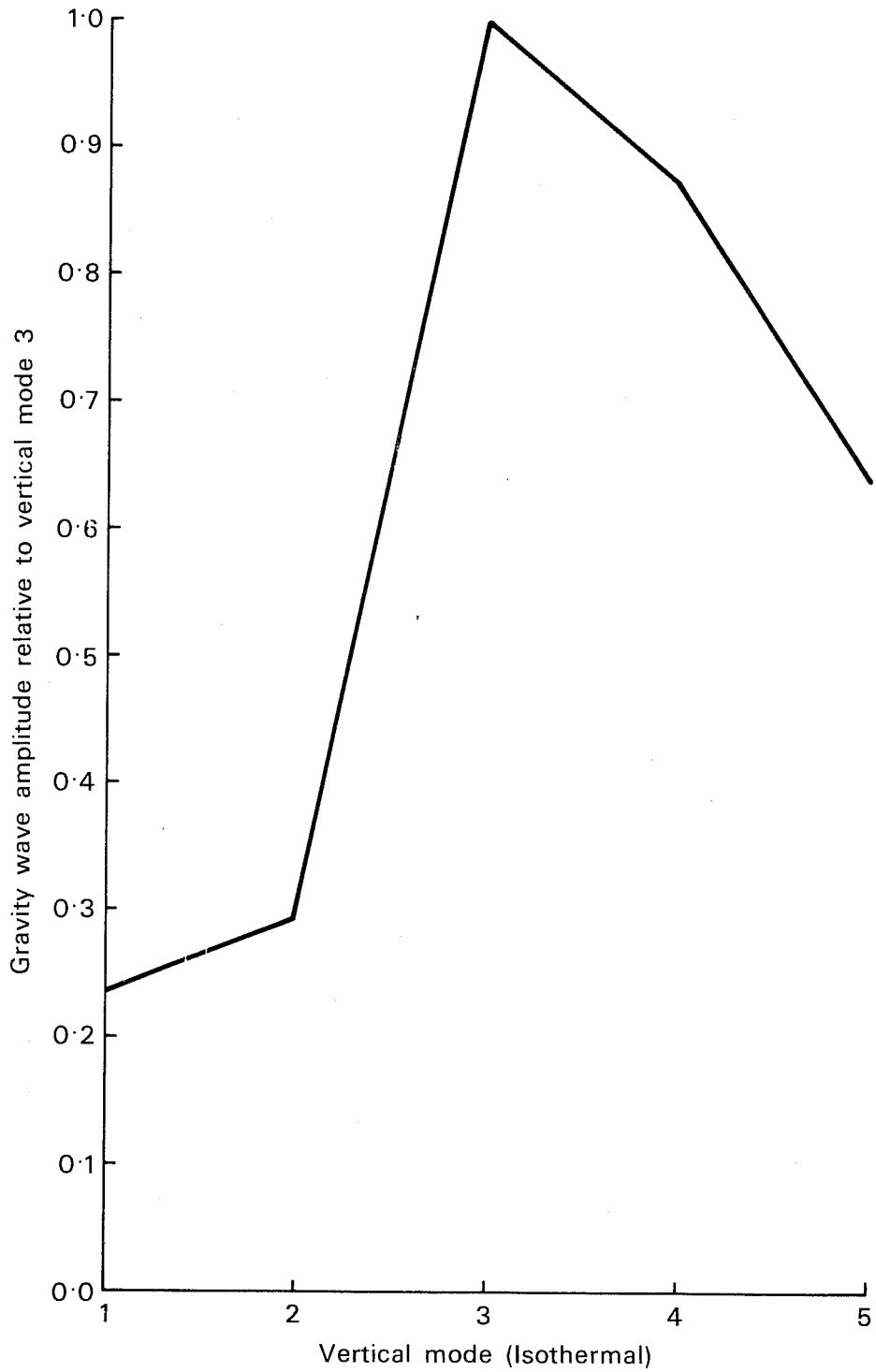
1·0
0·9
0·8
0·7
0·6
0·5
0·4
0·3
0·2
0·1
0·0
Gravity wave amplitude relative to vertical mode 3
1
2
3
4
5
Vertical mode (Isothermal)

Fig. 28

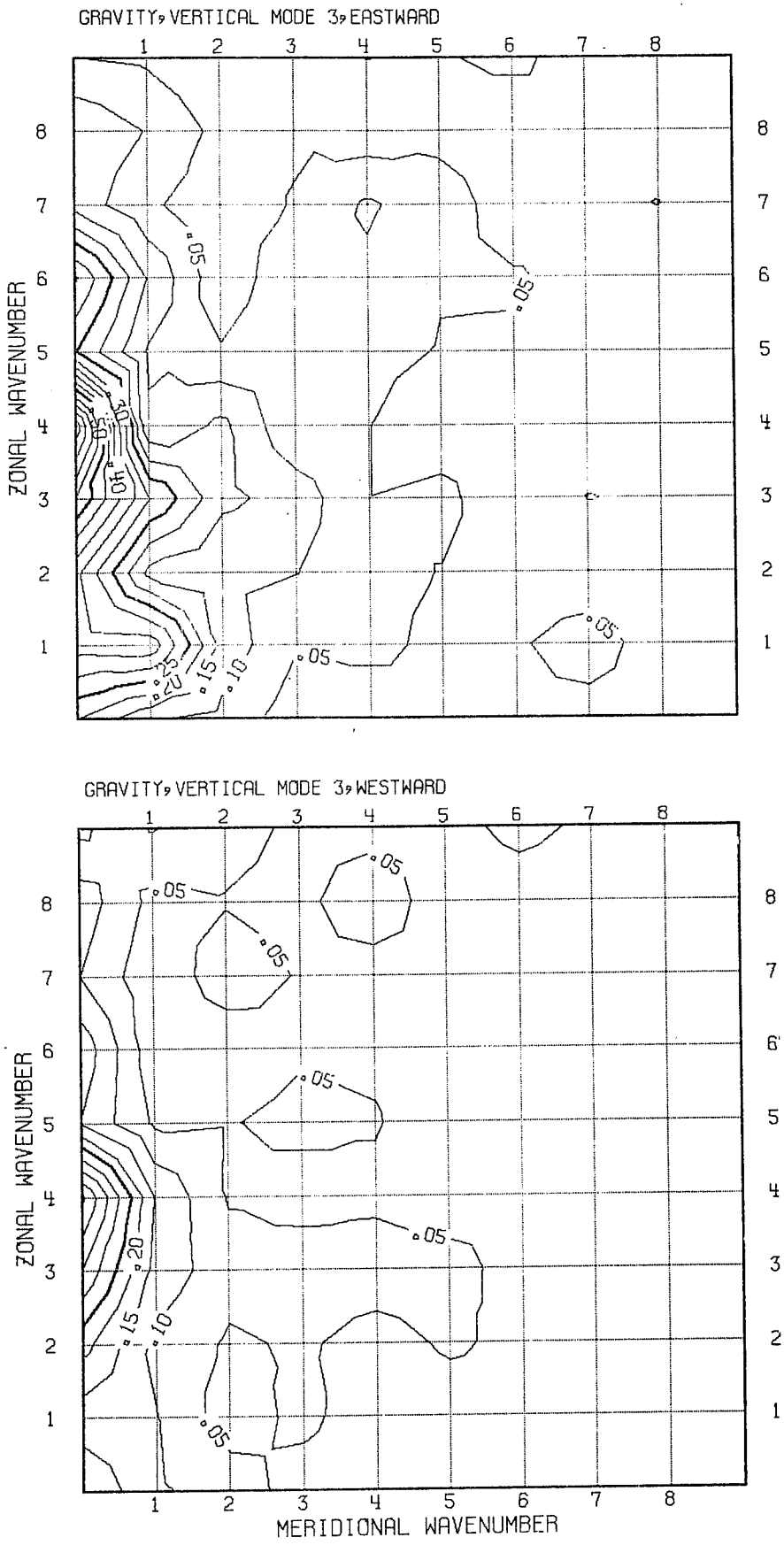

Fig. 29 Amplitudes of the eastward and westward inertia-gravity modes for vertical mode 3, for the mean differences 24 hour-6 hour of the March 1981 forecasts.

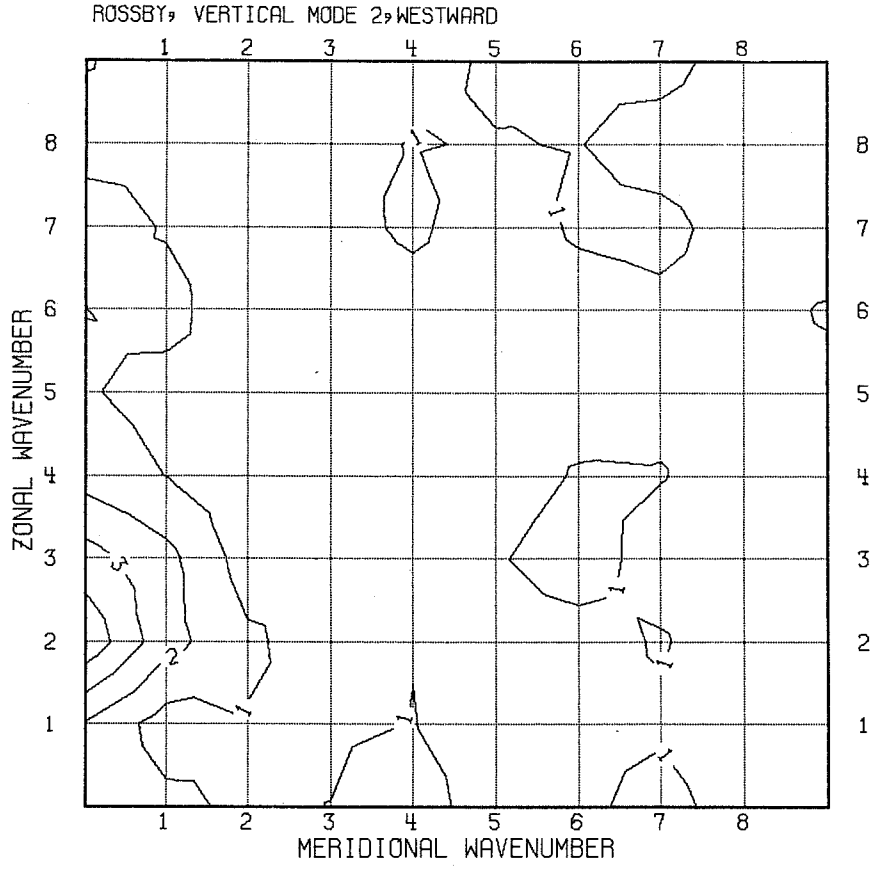

Fig. 30 As Fig. 29 but for the Rossby modes (including mixed mode).

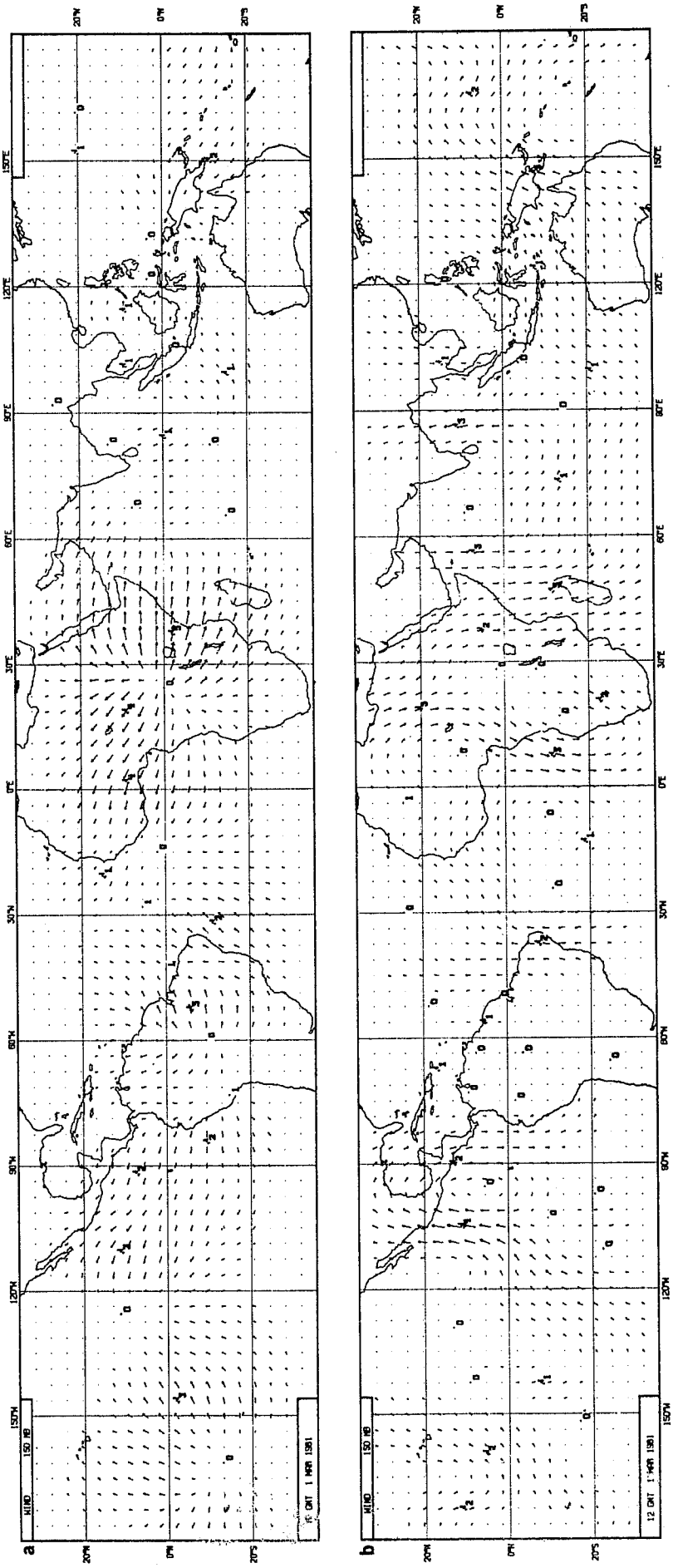

Fig. 31 a) The total inertia-gravity wave contribution (zonal wavenumber < 20) to the field shown in Fig. 26a.
b) As a) but for the Rossby waves (includes mixed mode).

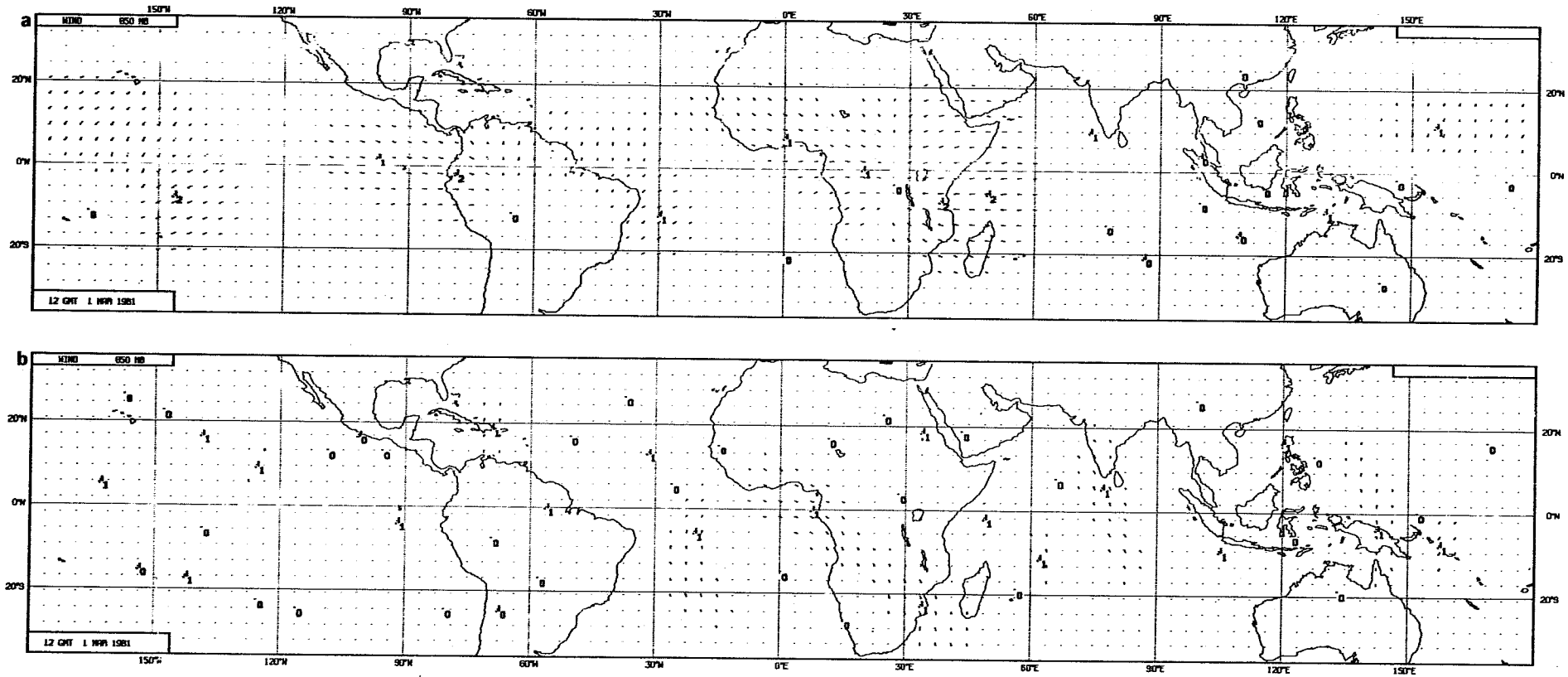

Fig. 32 a) The total inertia-gravity wave contribution (zonal wavenumber < 20) to the field shown in Fig. 26b.
b) As a) but for the Rossby waves (includes mixed mode).

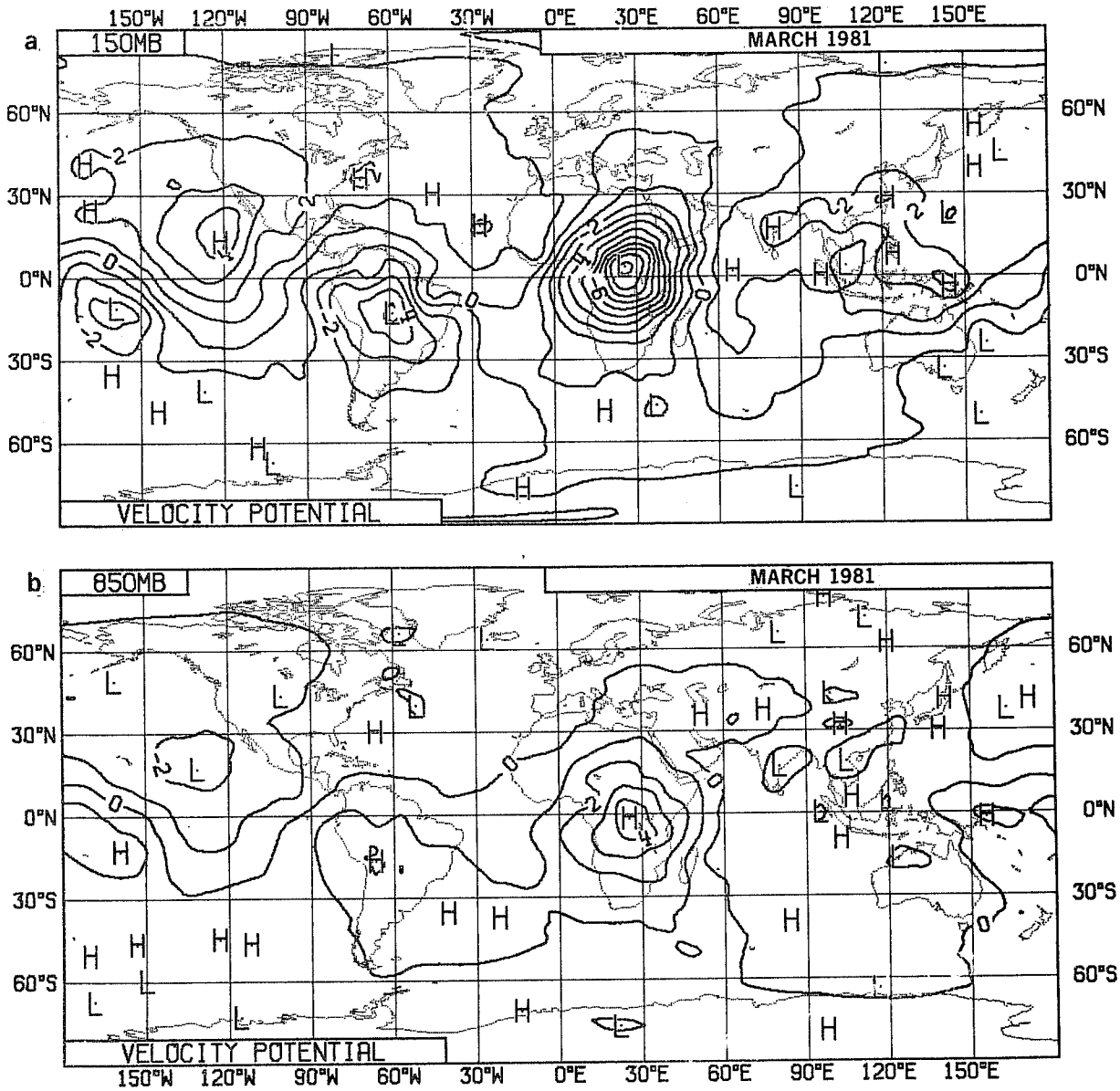

Fig. 33 Velocity potential field of the difference between the March mean 24 hour forecast and the March mean 6 hour forecast for 1981. a) 150 mb, b) 850 mb.

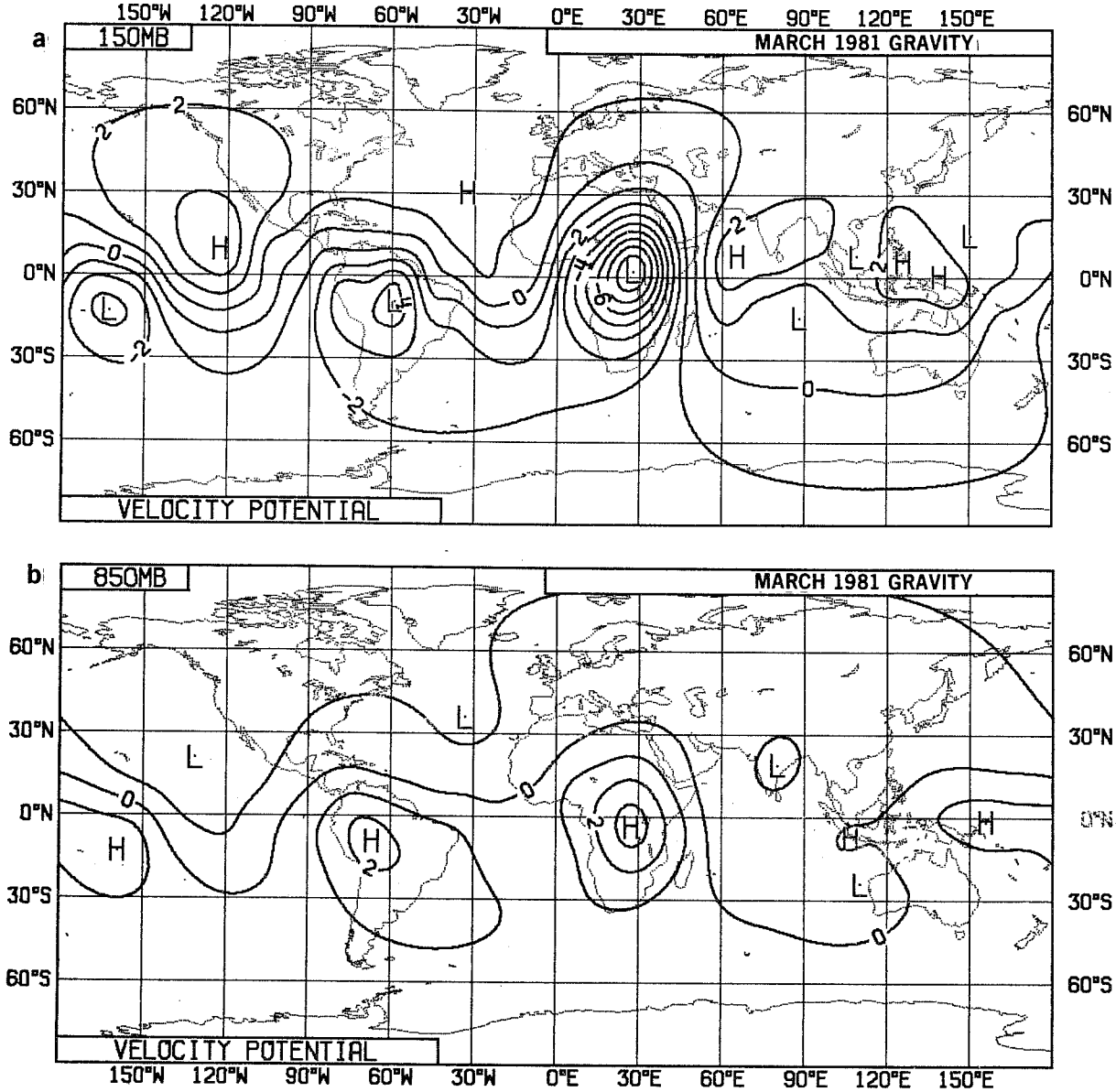

Fig. 34 The total inertia-gravity wave component (zonal wavenumber < 20) of the fields shown in Fig. 33. a) 150 mb, b) 850 mb.

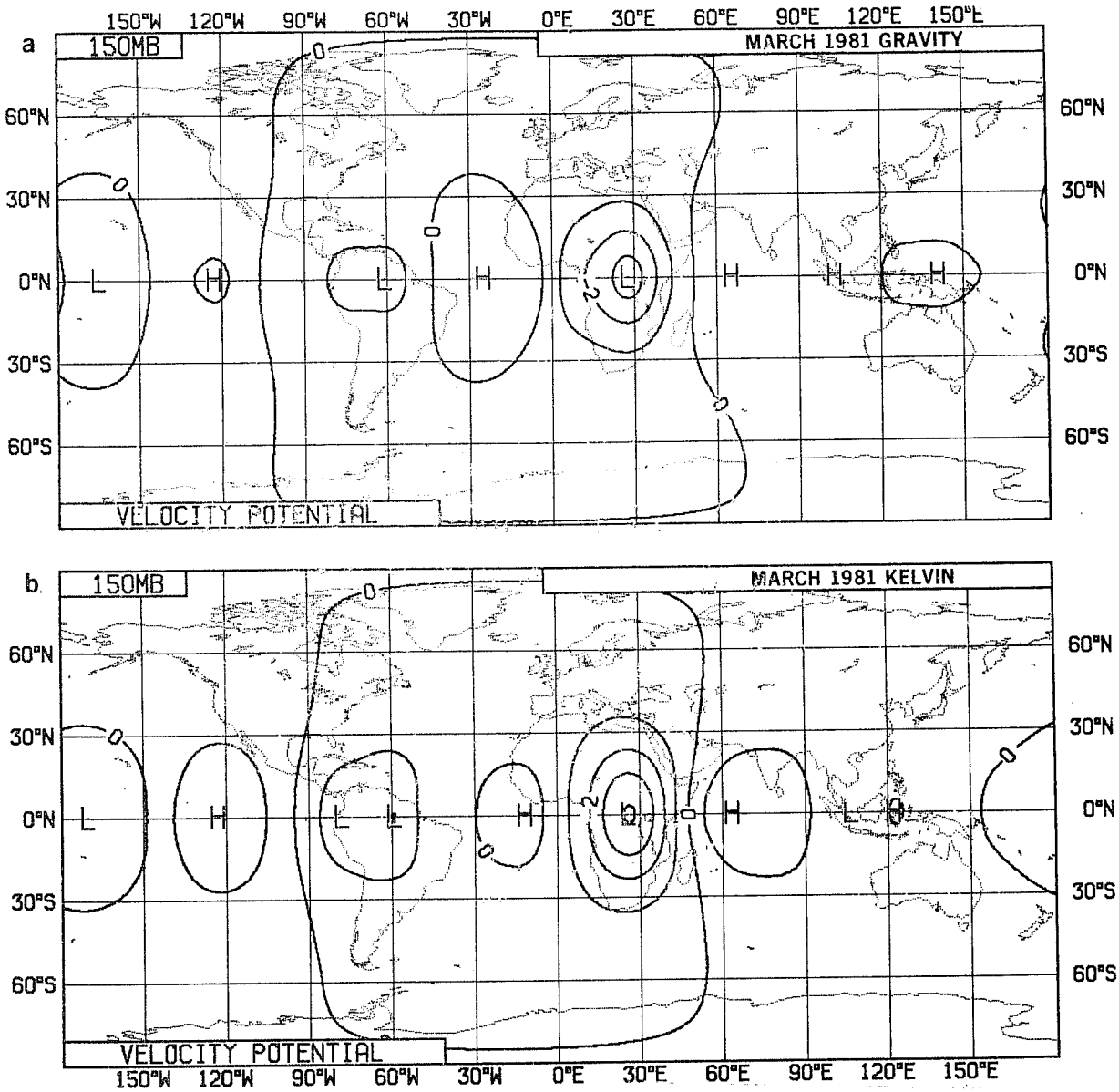

Fig. 35 a) The westward component of the inertia-gravity waves of Fig. 34a.
b) The eastward component of the inertia-gravity waves of Fig. 34a.

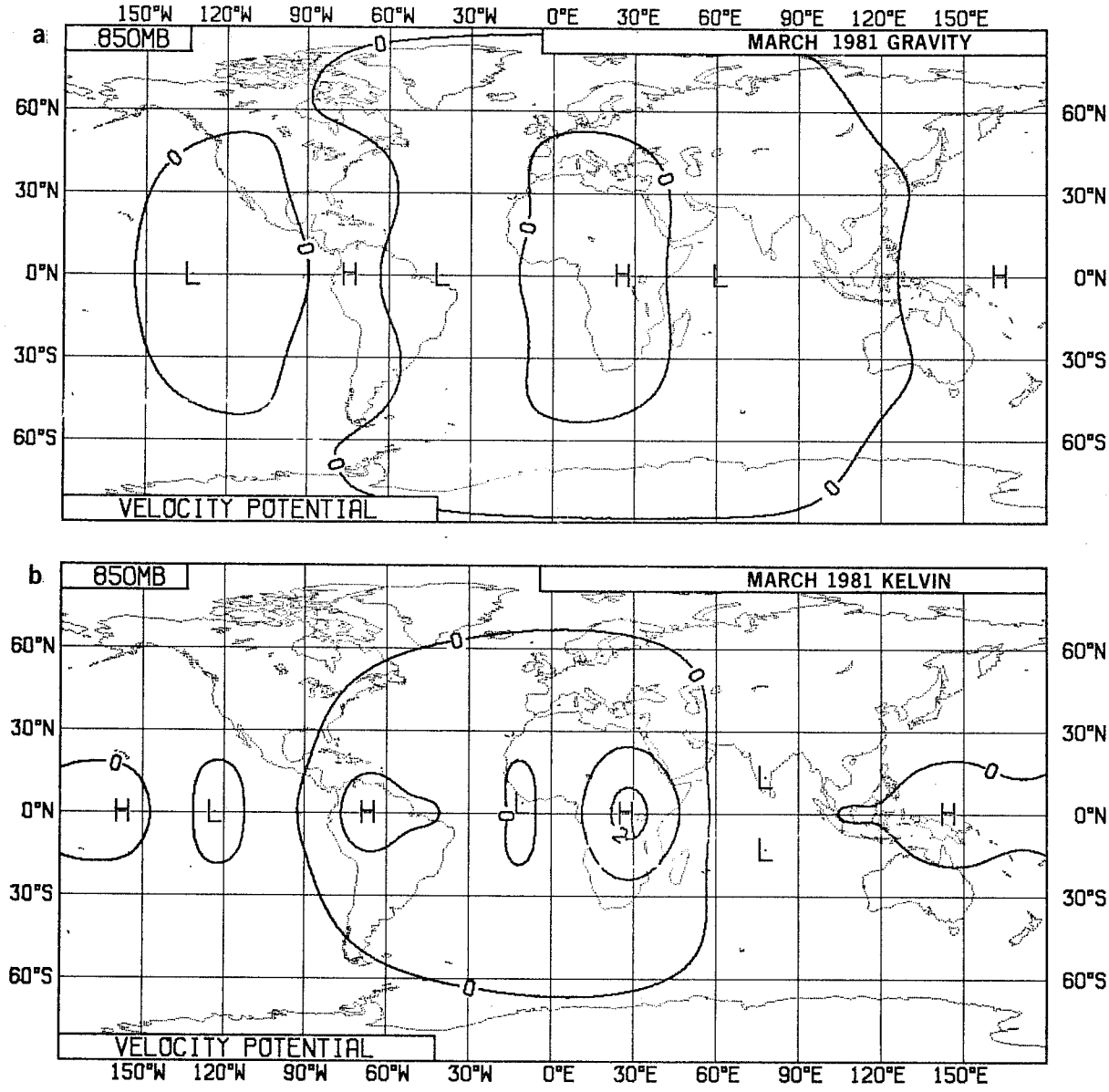

Fig. 36 As Fig. 35 but for 850 mb c.f. Fig. 34b.

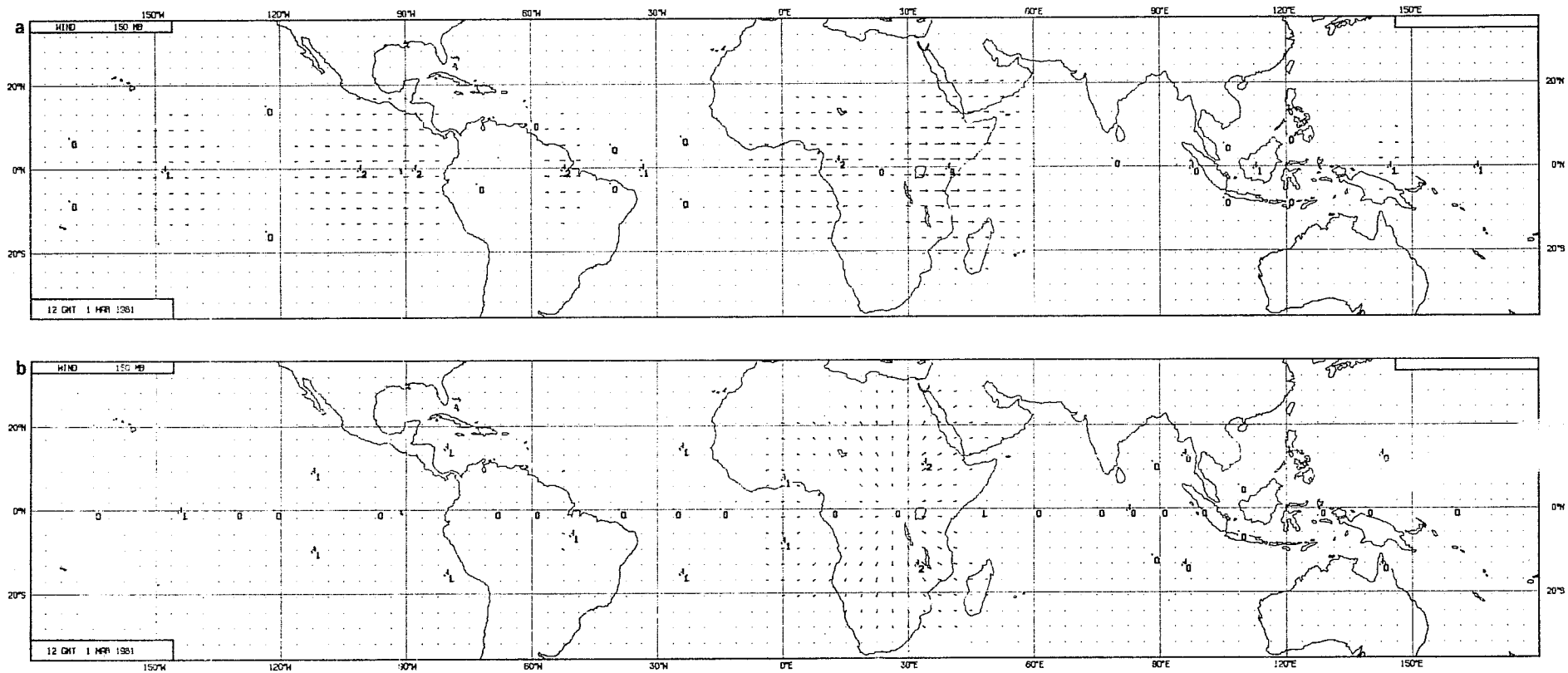

Fig. 37 a) The eastward component of the inertia-gravity waves of Fig. 32a. b) The westward component of the inertia-gravity waves of Fig. 32a.

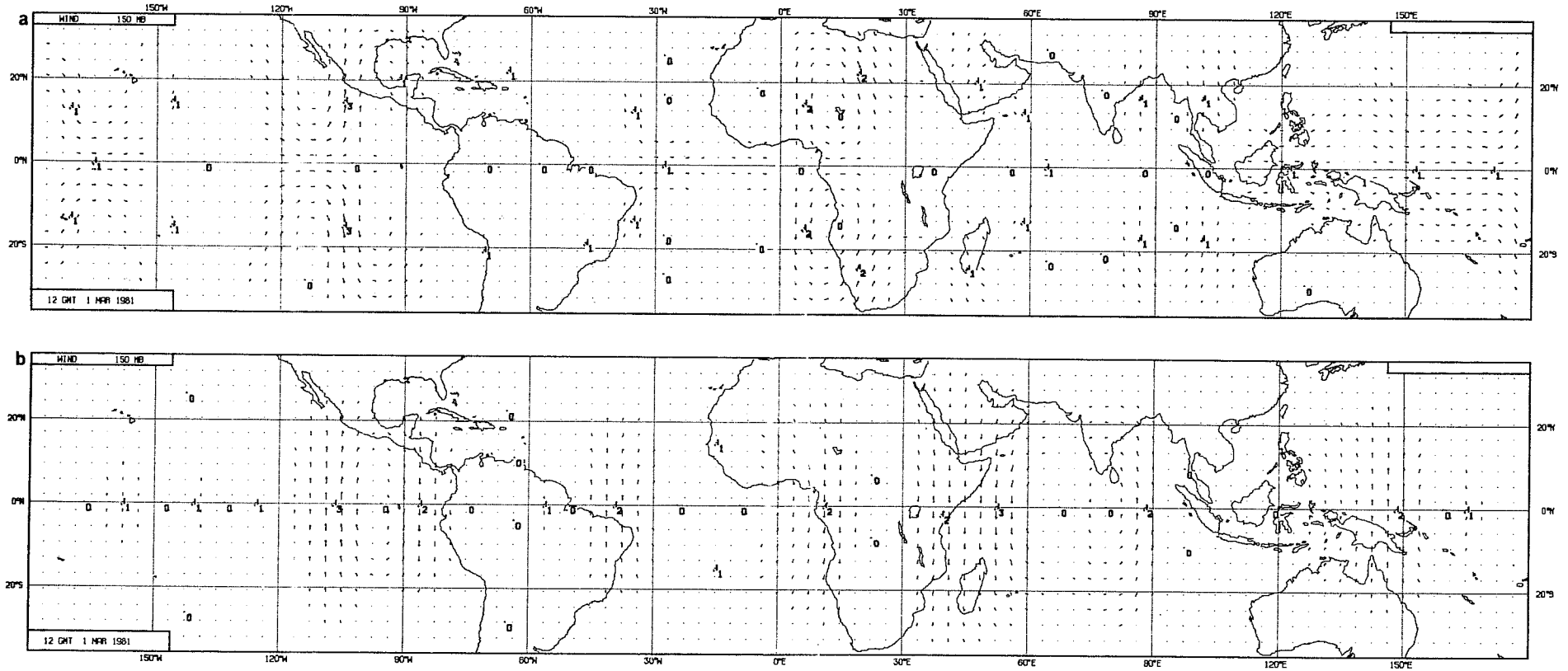

Fig. 38 a) The symmetric component of the Rossby wave of Fig. 32b. b) The antisymmetric component of the Rossby wave of Fig. 32b.

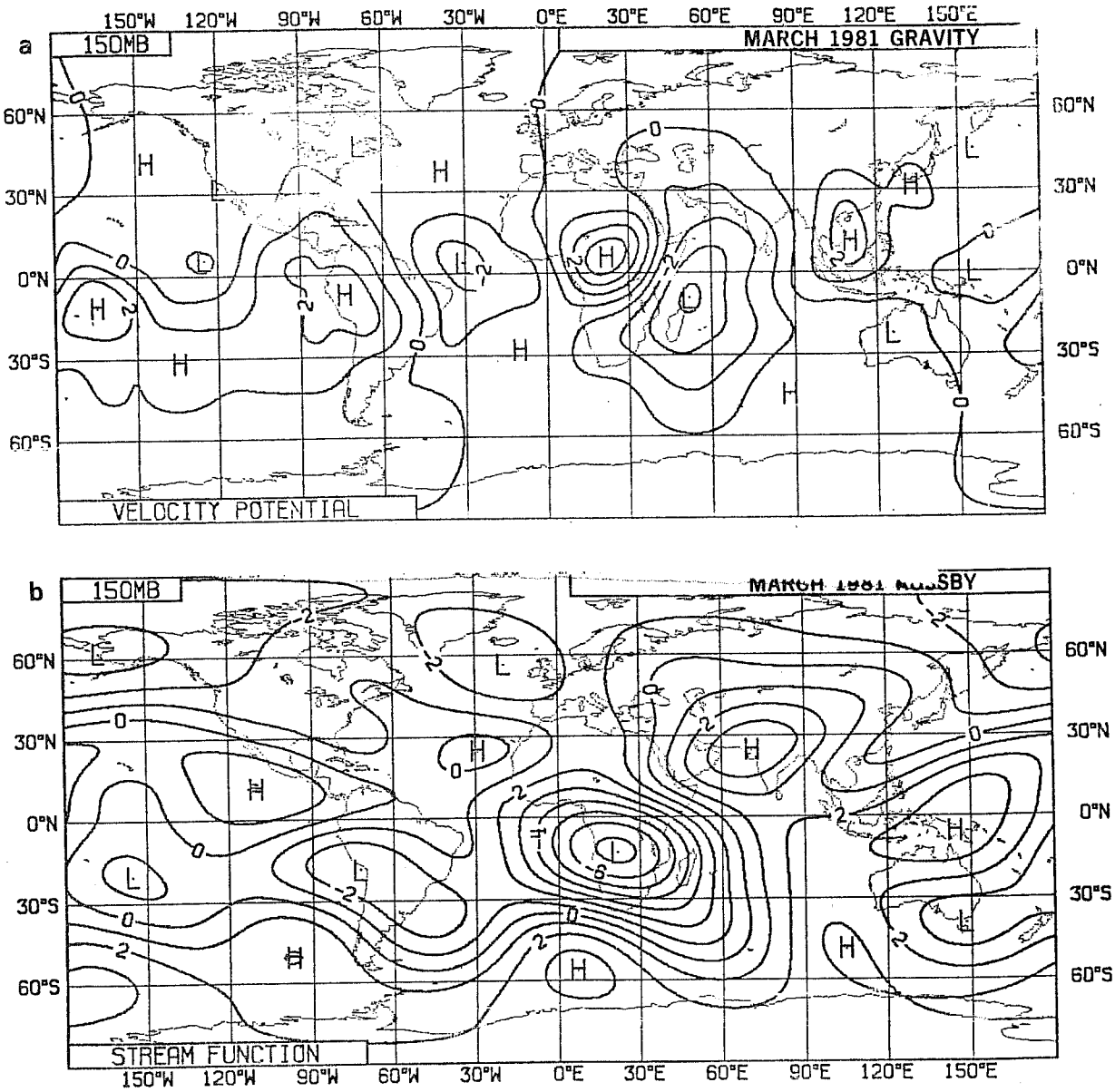

Fig. 39 March 1981 mean differences 48-24 hour. a) The gra... component, b) the Rossby wave component (including the mixed mode).

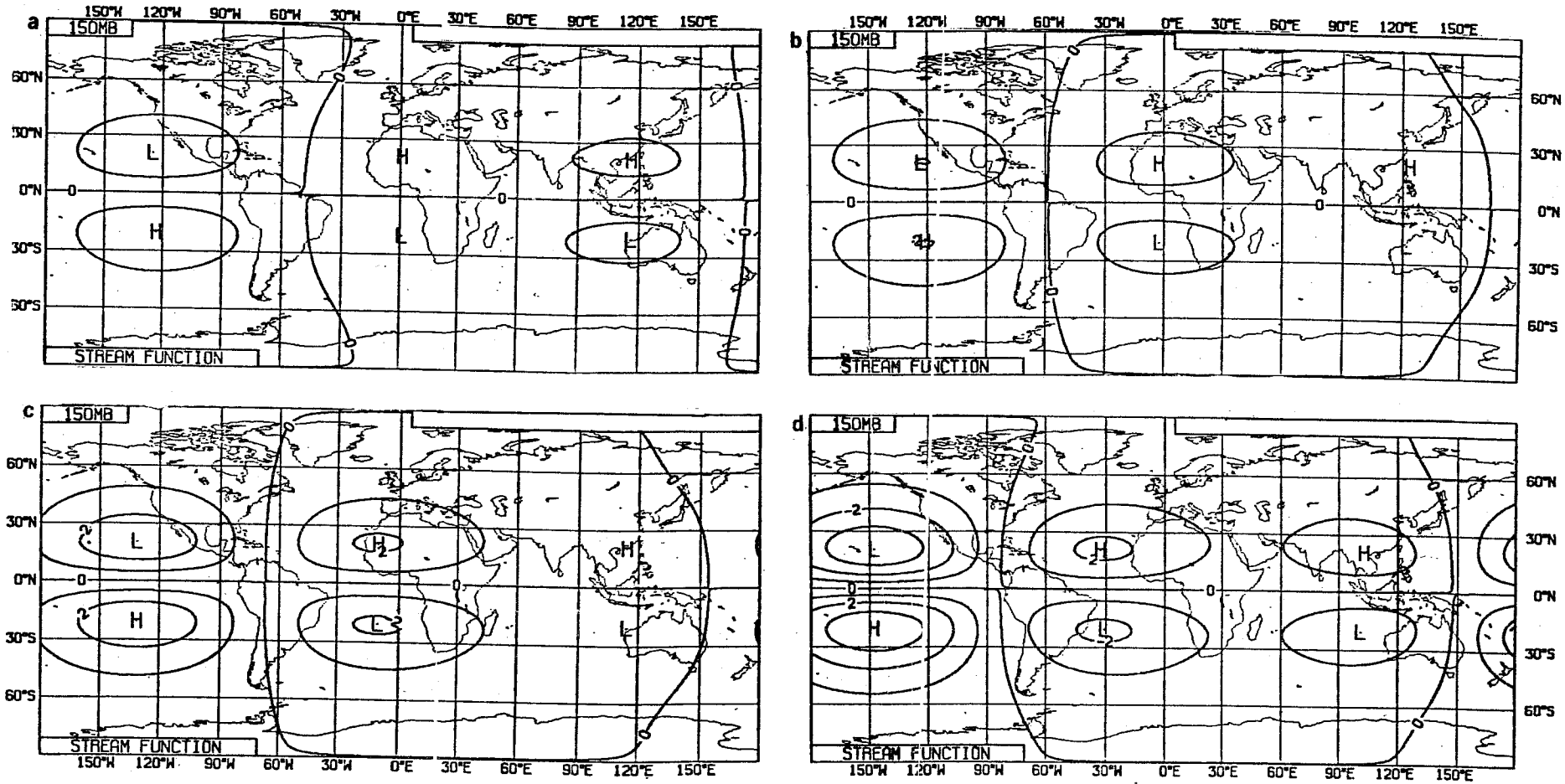

Fig. 40 March 1981 mean forecasts, the second internal symmetric Rossby mode component for a) 24 hour, b) 48 hour, c) 72 hour and d) 96 hour.